CHAPTER 2: REVIEW OF AERODYNAMIC FUNDAMENTALS

In this chapter a review is presented of those aerodynamic fundamentals which are important in understanding aircraft stability and control concepts. The assumption is made that the reader is reasonably familiar with fundamental aerodynamic theory such as discussed in Reference 2.1.

2.1 DEFINITION OF AIRFOIL PARAMETERS

The following geometric airfoil parameters have been found to be important in affecting aerodynamic characteristics of airfoils:

1) maximum thickness ratio, $(t/c)_{max}$
2) shape of the mean line (also referred to as camber). If the mean line is a straight line, the airfoil is said to be symmetrical.
3) leading edge shape or Δy parameter and leading edge radius (l.e.r.)
4) trailing edge angle, ϕ_{TE}

Figure 2.1 provides a geometric interpretation for these parameters.

The reader should consult Reference 2.2 for a detailed discussion of airfoil parameters and airfoil characteristics. Reference 2.2 also contains a large body of experimental data on a variety of NACA (National Advisory Committee on Aeronautics, predecessor of NASA, the National Aeronautics and Space Administration) airfoils. In addition, this reference contains explanations for the numerical designations used with NACA airfoils.

2.2 AIRFOIL AERODYNAMIC CHARACTERISTICS

Part VI of Reference 2.3 may be consulted for rapid empirical methods used to predict section lift, drag and pitching moment characteristics from the basic geometric parameters seen in Figure 2.1.

Figure 2.2 shows a typical graphical representation of those airfoil characteristics which are of prime importance in the analysis of airplane stability and control properties. Table 2.1 summarizes the principal effect of the geometric parameters of Figure 2.1 on the aerodynamic characteristics of Figure 2.2.

Because lifting surfaces (such as wings, tails, canards and pylons) can be thought of as spanwise arrangements of airfoils, the basic characteristics of airfoils have a major effect on the behavior of lifting surfaces. It is therefore important to be aware of those airfoil characteristics which have the potential of being 'driving' factors in airplane stability and control.

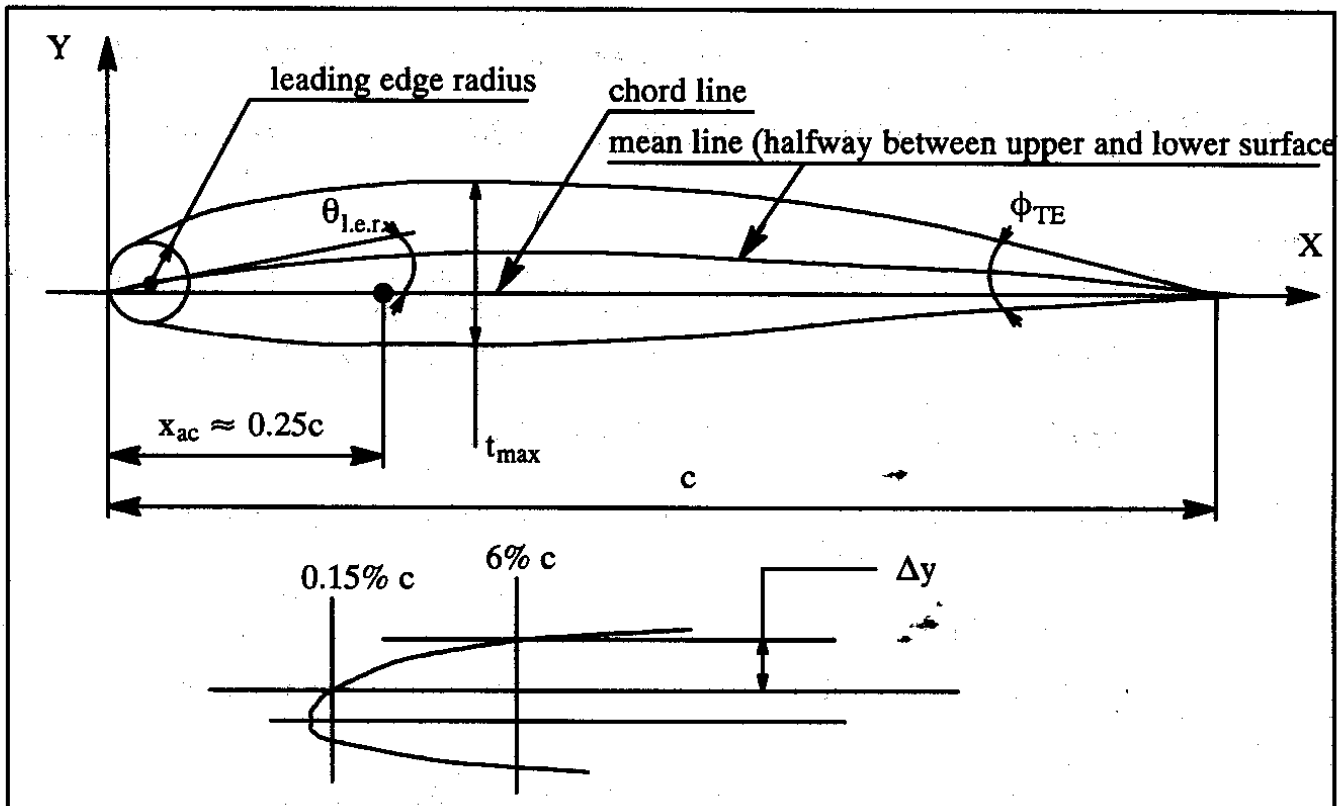

Figure 2.1 Definition of Important Airfoil Geometric Parameters

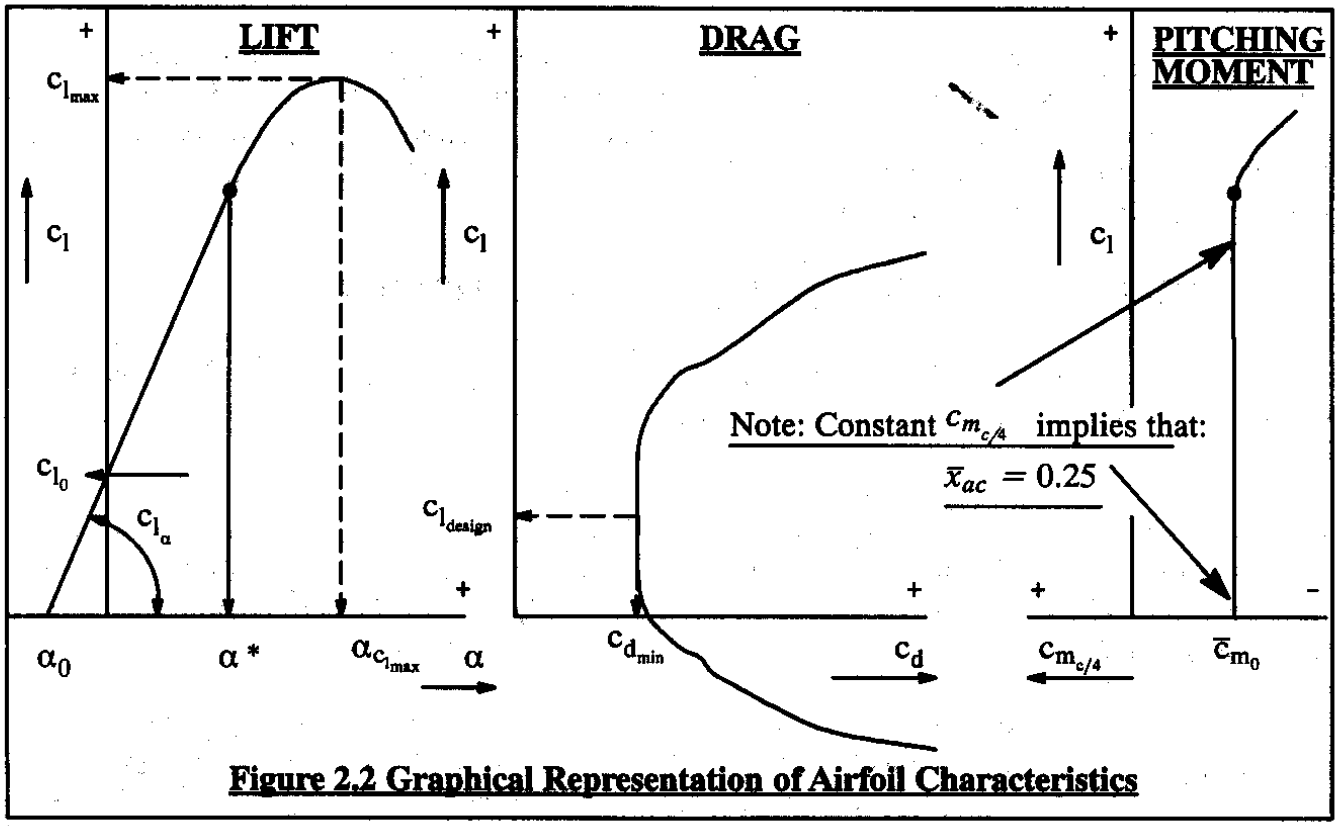

Figure 2.2 Graphical Representation of Airfoil Characteristics

Table 2.1 Summary of Principal Effects of Geometric Airfoil Parameters on Aerodynamic characteristics of Airfoils

Geometric Airfoil Parameter	Principal Effect on Aerodynamic Characteristics other than Drag
Maximum Thickness ratio, t/c_{max}	Maximum lift coefficient, $c_{l_{max}}$ Aerodynamic center, $\bar{x}_{ac} = \frac{x_{ac}}{c}$
Shape of the mean line	Zero lift angle of attack, α_0 Maximum lift coefficient, $c_{l_{max}}$ Pitching moment coefficient at zero lift coefficient, $\bar{c}_{m_0}$
Leading edge radius, l.e.r. and leading edge shape parameter, Δy	Maximum lift coefficient, $c_{l_{max}}$ and end of the linear angle of attack range, α^*
Trailing edge angle, ϕ_{TE}	Aerodynamic center, $\bar{x}_{ac} = \frac{x_{ac}}{c}$

Note: References 2.2 and Part VI of 2.3 should be consulted for theoretical, empirical and experimental details.

The following airfoil (two–dimensional) properties of Figure 2.2 will have a significant effect on their lifting surface (three–dimensional) counterparts.

In Lift:
* angle of attack for zero lift: α_0
* lift curve slope: c_{l_α}
* maximum lift coefficient: $c_{l_{max}}$ (function of Reynolds Number, R_N)
* angle of attack at $c_{l_{max}}$, $\alpha_{c_{l_{max}}}$
* end of the linear angle of attack range: α^*

In Drag:
* lift coefficient for minimum drag or design lift coefficient: $c_{l_{design}}$
* minimum drag coefficient: $c_{d_{min}}$ (function of R_N)

In Pitching Moment:
* pitching moment coefficient at zero lift coefficient: $\bar{c}_{m_0}$
* aerodynamic center (i.e. that point on the airfoil chord where the variation of pitching moment coefficient with angle of attack is zero). Figure 2.3 shows how the aerodynamic center is located geometrically. The following notation is normally used: $\bar{x}_{ac} = \frac{x_{ac}}{c}$

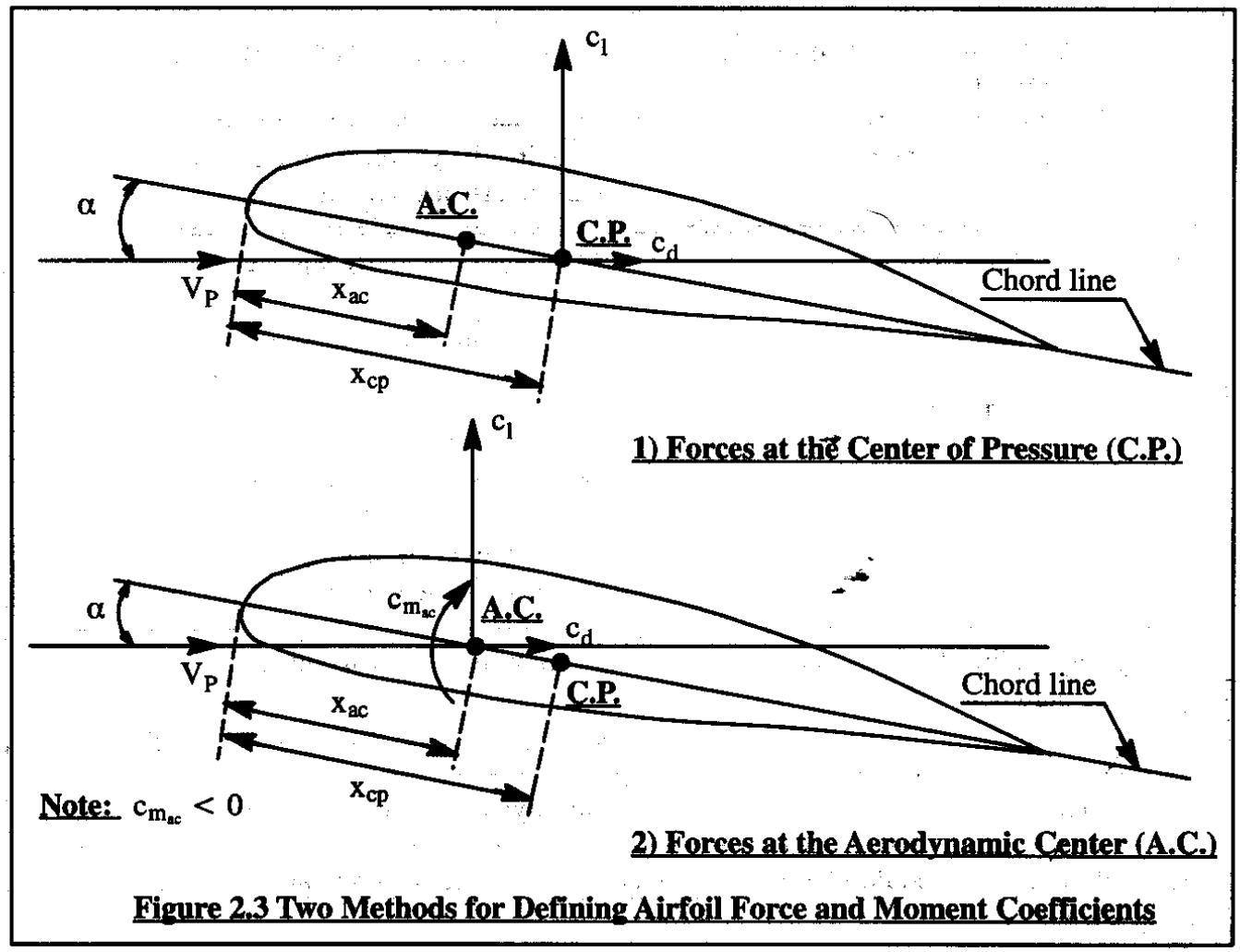

Figure 2.3 Two Methods for Defining Airfoil Force and Moment Coefficients

Table 2.2 gives an overview of typical numerical values associated with some of these quantities. It will be noted that the airfoil lift–curve–slope, c_{l_α} typically has a value of approximately 2π (roughly 6.3 per rad or 0.110 per deg). Note also that the location of airfoil aerodynamic center is typically close to the quarter chord point: $\bar{x}_{ac} = 0.25$. The reader should be aware of the fact that most of these quantities are also a strong function of Mach Number, M. The dependence on Mach Number of the aerodynamic center location, $\bar{x}_{ac}$ and the lift–curve–slope c_{l_α} of airfoils is of particular significance to airplane stability and control. For that reason these characteristics are discussed in more detail in Sub–sections 2.2.1 and 2.2.2 respectively.

2.2.1 AIRFOIL AERODYNAMIC CENTER

Definition: The aerodynamic center of an airfoil is defined as that point on its chord about which the pitching moment coefficient is invariant with angle of attack.

In other words: $\bar{x}_{ac} = \frac{x_{ac}}{c}$ is that point for which: $c_{m_\alpha} = 0$. The aerodynamic center of an airfoil should not be confused with its center of pressure.

Table 2.2 Experimental, Low Speed NACA Airfoil Data for Smooth Leading Edges
(Note: Data reproduced from Reference 2.1 for $R_N = 9 \times 10^6$)

Airfoil	α_0 (deg)	$\bar{c}_{m_0}$	c_{l_α} (1/deg)	$\bar{x}_{ac}$	$\alpha_{c_{l_{max}}}$ (deg)	$c_{l_{max}}$	α^* (deg)
0006	0	0	0.108	0.250	9.0	0.92	9.0
0009	0	0	0.109	0.250	13.4	1.32	11.4
1408	0.8	–0.023	0.109	0.250	14.0	1.35	10.0
1410	–1.0	–0.020	0.108	0.247	14.3	1.50	11.0
1412	–1.1	–0.025	0.108	0.252	15.2	1.58	12.0
2412	–2.0	–0.047	0.105	0.247	16.8	1.68	9.5
2415	–2.0	–0.049	0.106	0.246	16.4	1.63	10.0
2418	–2.3	–0.050	0.103	0.241	14.0	1.47	10.0
2421	–1.8	–0.040	0.103	0.241	16.0	1.47	8.0
2424	–1.8	–0.040	0.098	0.231	16.0	1.29	8.4
23012	–1.4	–0.014	0.107	0.247	18.0	1.79	12.0
23015	–1.0	–0.007	0.107	0.243	18.0	1.72	10.0
23018	–1.2	–0.005	0.104	0.243	16.0	1.60	11.8
23021	–1.2	0	0.103	0.238	15.0	1.50	10.3
23024	–0.8	0	0.097	0.231	15.0	1.40	9.7
64–006	0	0	0.109	0.256	9.0	0.80	7.2
64–009	0	0	0.110	0.262	11.0	1.17	10.0
64_1–012	0	0	0.111	0.262	14.5	1.45	11.0
64_1–212	–1.3	–0.027	0.113	0.262	15.0	1.55	11.0
64_1–412	–2.6	–0.065	0.112	0.267	15.0	1.67	8.0
64–206	–1.0	–0.040	0.110	0.253	12.0	1.03	8.0
64–209	–1.5	–0.040	0.107	0.261	13.0	1.40	8.9
64–210	–1.6	–0.040	0.110	0.258	14.0	1.45	10.8
64A010	0	0	0.110	0.253	12.0	1.23	10.0
64A210	–1.5	–0.040	0.105	0.251	13.0	1.44	10.0
64A410	–3.0	–0.080	0.100	0.254	15.0	1.61	10.0
64_1A212	–2.0	–0.040	0.100	0.252	14.0	1.54	11.0
64_2A215	–2.0	–0.040	0.095	0.252	15.0	1.50	12.0

Note: For definition of symbols, see Figure 2.2 and the list of Symbols

Definition: The center of pressure of an airfoil is that point on its chord where the resultant of the pressure distribution (resultant aerodynamic force) acts.

The lift distribution on any non–symmetrical (cambered) airfoil can be shown to be the sum of two types of lift distribution:

1.) the basic lift distribution which depends on the shape (camber) of the mean line. This basic lift distribution has zero net lift but non–zero pitching moment: $\bar{c}_{m_0} < 0$ for airfoils with positive camber.

2.) the additional lift distribution which depends linearly on the angle of attack, α. The net lift of an airfoil is due to this additional lift distribution.

Apparently, the aerodynamic center of an airfoil can also be thought of as the centroid of the additional lift distribution. Therefore, for a symmetrical airfoil the center of pressure and the aerodynamic center coincide!

Figure 2.3 presents two methods used to resolve the force and moment coefficients which act on an airfoil. In this text the second method will be used. Expressing the center of pressure and aerodynamic center locations relative to the leading edge of the airfoil as: x_{ac} and x_{cp} respectively it is found that for small angles of attack and for negligible drag contribution to the pitching moment:

$$c_{m_{ac}} = -c_l(x_{cp} - x_{ac})/c \tag{2.1}$$

From this the location of the airfoil center of pressure can be solved:

$$x_{cp} = x_{ac} - (c_{m_{ac}}c)/(c_l) \tag{2.2}$$

Because the quantity $c_{m_{ac}}$ is negative for positively cambered airfoils, the center of pressure is behind the aerodynamic center. Note that:

$$c_{m_{ac}} = \bar{c}_{m_0} \tag{2.3}$$

Because a symmetrical airfoil has no net pitching moment at zero lift: $c_{m_{ac}} = 0$. As
symm.airfoil

a consequence, for a symmetrical airfoil: $x_{ac} = x_{cp}$. Do not forget that this property does **NOT** apply to cambered (un–symmetrical airfoils).

The data in Table 2.2 indicate that the aerodynamic center location for airfoils is roughly at the quarter chord. Actually, the airfoil thickness ratio and trailing edge angle together define where the aerodynamic center is located. Figure 2.4 (reproduced from Reference 2.4) shows this. Note that the data in Figure 2.4 straddle the 25% chord location!

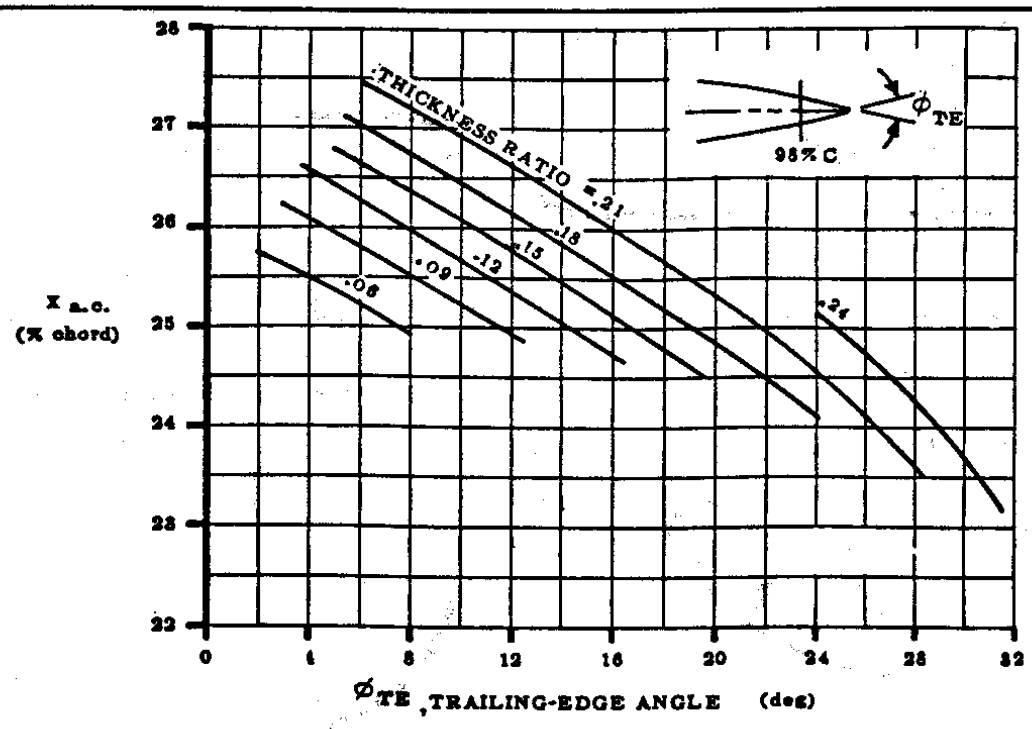

Figure 2.4 Effect of Trailing Edge Angle and Thickness Ratio on Airfoil Aerodynamic Center Location (Reproduced from Ref. 2.4)

As the Mach Number increases from low sub sonic to transonic the airfoil center of pressure and aerodynamic center tend to move aft (not necessarily at the same rate). For a thin, symmetrical airfoil at exactly M=1 the center of pressure tends to be at the semi–chord (50%) position. An example of how the aerodynamic center moves aft with Mach Number is shown in Figure 2.5. This aft shift of the aerodynamic center will be shown (Chapters 4 and 5) to have significant consequences to the stability and controllability of airplanes.

2.2.2 AIRFOIL LIFT CURVE SLOPE

According to thin airfoil theory, the lift–curve slope of an airfoil, c_{l_α} increases with Mach Number in the subsonic speed range as follows:

$$c_{l_{\alpha_M}} = \frac{c_{l_{\alpha_{M=0}}}}{\sqrt{1 - M^2}} \qquad (2.4)$$

This in accordance with the so–called Prandtl–Glauert transformation as explained in detail in Reference 2.5 (pages 200–203). Figure 2.5 shows a graphical representation of Eqn.(2.4). According to Reference 2.6 (Chapter 3), in the supersonic speed range this relationship becomes:

$$c_{l_{\alpha_M}} = \frac{4}{\sqrt{M^2 - 1}} \qquad (2.5)$$

Note that both Equations (2.4) and (2.5) predict the lift–curve slope to extend to infinity around M=1.0. This does not happen in reality because the theories used to derive these equations become invalid in the Mach range around M=1.0. The 'faired' curve shown in Figure 2.5 represents more closely what really happens.

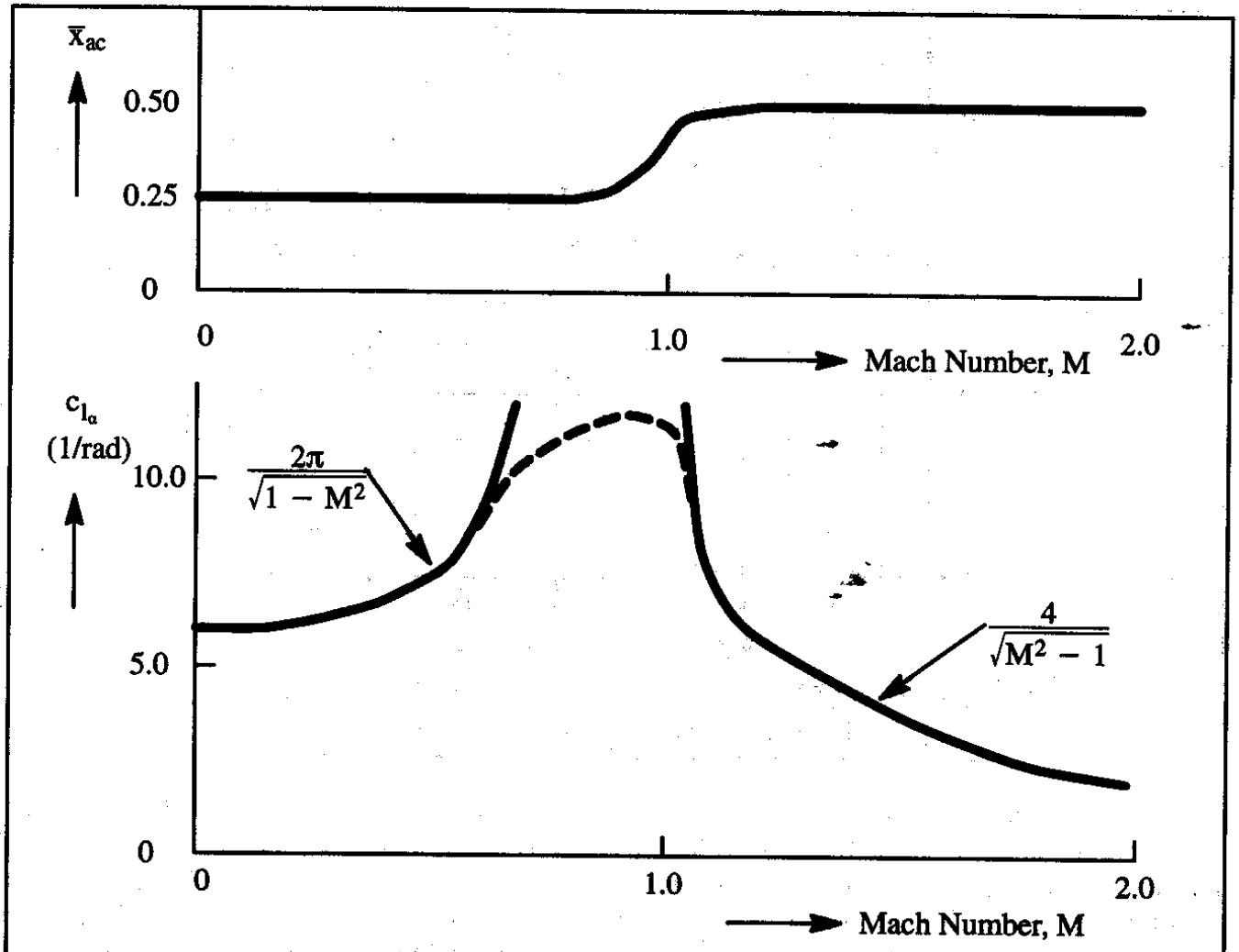

Figure 2.5 Effect of Mach Number on Airfoil Aerodynamic Center and Lift Curve Slope

2.3 PLANFORM PARAMETERS

As indicated before, airfoils are integrated in a spanwise manner to form lifting surfaces such as wings, tails, canards and pylons. The planform geometry of these lifting surfaces plays a major role in determining their aerodynamic characteristics. In the following it is assumed that most of these planforms can be approximated by a so–called straight tapered form as shown in Figure 2.6. The following planform quantities are important in stability and control analyses:

$$\text{Taper ratio, } \lambda = \frac{c_t}{c_r} \tag{2.6}$$

$$\text{Aspect ratio, } A = \frac{b^2}{S} = \frac{2b}{c_r(1 + \lambda)} \tag{2.7}$$

$$\text{Area, } S = \frac{b}{2}c_r(1 + \lambda) \tag{2.8}$$

$$\text{Mean geometric chord (mgc), } \bar{c} = \frac{2}{3}c_r\left(\frac{1 + \lambda + \lambda^2}{1 + \lambda}\right) \tag{2.9}$$

Lateral location of the mgc, $y_{mgc} = \frac{b(1 + 2\lambda)}{6(1 + \lambda)}$ (2.10)

Longitudinal location of the mgc, $x_{mgc} = \frac{b(1 + 2\lambda)}{6(1 + \lambda)} \tan \Lambda_{LE}$ (2.11)

Sweep Angle of the n fraction locus: $\tan \Lambda_n = \tan \Lambda_{LE} - \frac{4n(1 - \lambda)}{A(1 + \lambda)}$ (2.12)

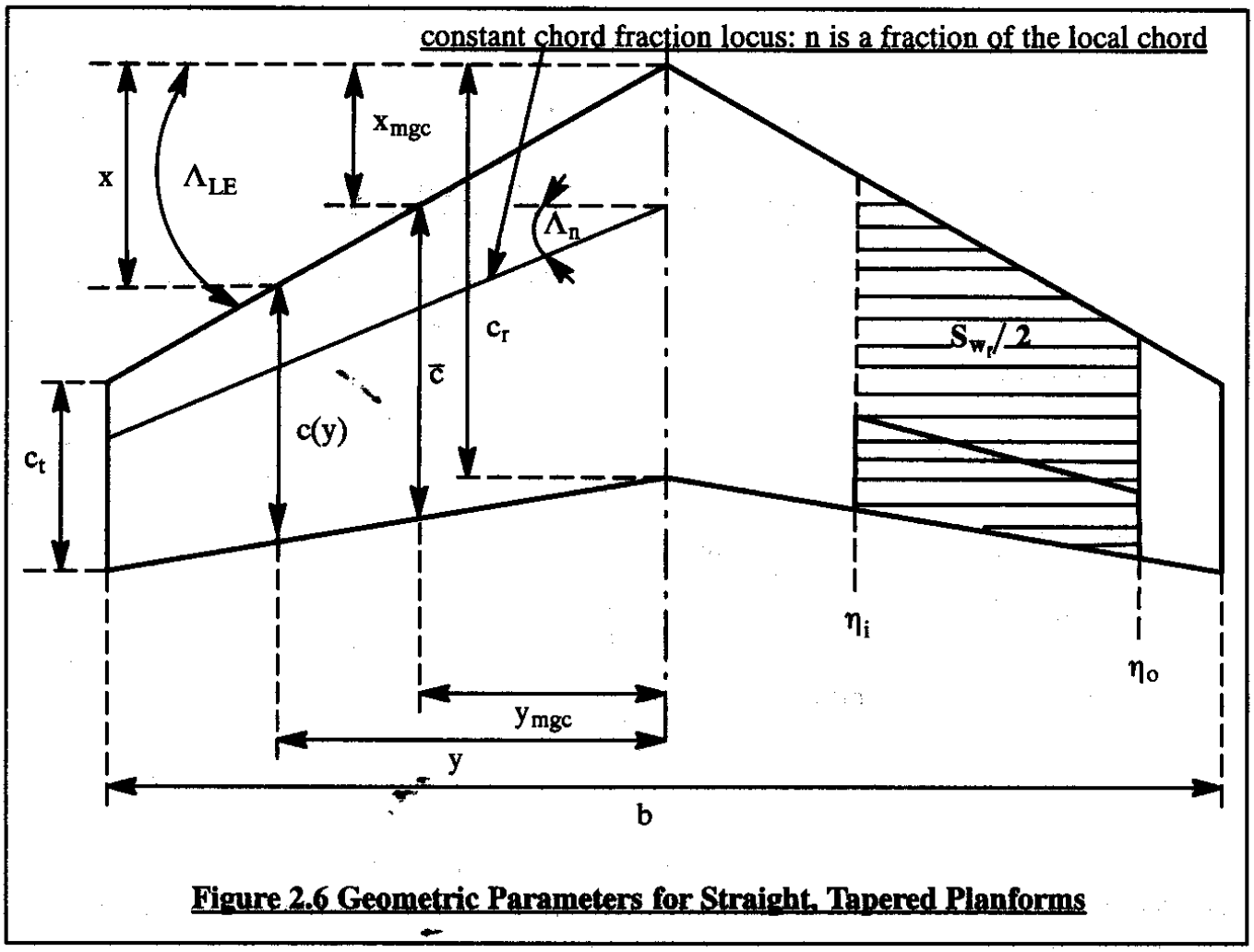

Figure 2.6 Geometric Parameters for Straight, Tapered Planforms

For a more general planform, the following integrals can be used to determine the length and location of the mean geometric chord:

Mean geometric chord: $\bar{c} = \frac{1}{S} \int_{-b/2}^{+b/2} c^2(y)dy$ (2.13)

Lateral location of the mgc, $y_{mgc} = \frac{2}{S} \int_{-b/2}^{+b/2} yc(y)dy$ (2.14)

$$\text{Longitudinal location of the mgc, } x_{mgc} = \frac{1}{S}\int_{-b/2}^{+b/2} xc(y)dy \tag{2.15}$$

Many lifting surfaces are equipped with trailing edge flaps and /or trailing edge control surfaces. The inboard and outboard stations of flaps and/or control surfaces are identified by semi–span fractions called η_i and η_o respectively. Such flaps and/or control surfaces affect an area of the planform called the flapped wing area, S_{w_f} :

$$S_{w_f} = S\frac{(\eta_o - \eta_i)}{(1 + \lambda)}\left\{2 - (1 - \lambda)(\eta_i + \eta_o)\right\} \tag{2.16}$$

2.4 COEFFICIENTS AND REFERENCE GEOMETRIES

In airplane stability and control, the following dimensionless aerodynamic coefficients are used frequently:

$$\text{Lift coefficient: } C_L = \frac{L}{\bar{q}S} \tag{2.17}$$

$$\text{Drag coefficient: } C_D = \frac{D}{\bar{q}S} \tag{2.18}$$

$$\text{Side force coefficient: } C_y = \frac{F_{A_y}}{\bar{q}S} \tag{2.19}$$

$$\text{Rolling moment coefficient: } C_l = \frac{L_A}{\bar{q}Sb} \tag{2.20}$$

$$\text{Pitching moment coefficient: } C_m = \frac{M_A}{\bar{q}S\bar{c}} \tag{2.21}$$

$$\text{Yawing moment coefficient: } C_n = \frac{N_A}{\bar{q}Sb} \tag{2.22}$$

It is important to always identify the reference geometries used when presenting and/or discussing aerodynamic data! For the moment coefficients, the location of the moment reference center must also be identified!

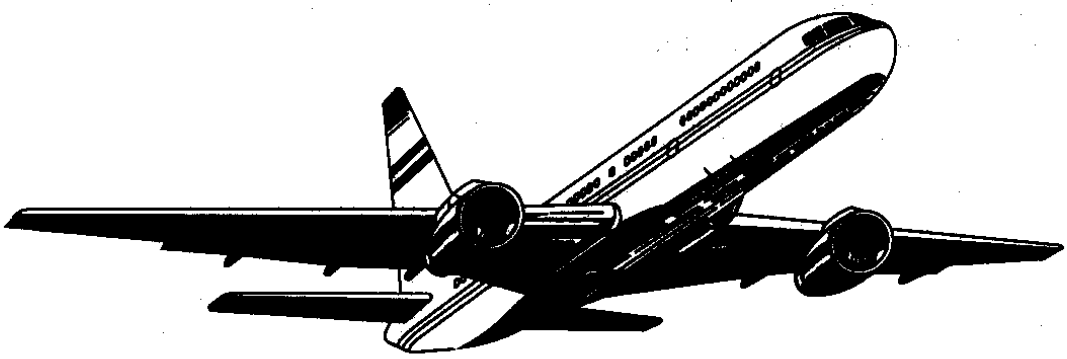

2.5 AERODYNAMIC CHARACTERISTICS OF PLANFORMS AND FUSELAGE

In this section a very condensed discussion is presented of those aerodynamic characteristics of planforms which are of major concern in the prediction and analysis of airplane stability and control behavior. These characteristics are:

2.5.1 Lift–curve slope, C_{L_α}

2.5.2 Aerodynamic center, x_{ac}

2.5.3 Zero–lift angle of attack, α_0

2.5.4 Moment coefficient about the aerodynamic center, $C_{m_{ac}}$

2.5.5 Downwash (and upwash), ε and its rate of change with angle of attack, $d\varepsilon/d\alpha$

2.5.6 Effect of the fuselage on planform aerodynamic center,

All characteristics discussed in this section apply to a variety of lifting surfaces such as: wings, horizontal tails, canards, vertical tails, pylons, etc. To distinguish the aerodynamic characteristics of one lifting surface from another, subscripts are used. The following subscripts are used:

w for wing	h for horizontal tail	p for pylon
c for canard	v for vertical tail	s for store

2.5.1 LIFT–CURVE SLOPE

The lift–curve slope of planforms, C_{L_α} has been found to depend primarily on the following parameters:

* Aspect ratio	* Sweep angle	* Taper ratio
* Section lift–curve slope		* Mach number

Part VI of Reference 2.3 contains methods for estimating planform C_{L_α} values (Pages 248–255). These methods have been programmed in the Advanced Aircraft Analysis (AAA) program which is described in Appendix A. Figure 2.7 shows how planform lift–curve slope varies with Mach number, sweep angle and aspect ratio. Note the following behaviors:

In the subsonic to transonic speed range:

* C_{L_α} increases with increasing aspect ratio
* C_{L_α} decreases with increasing sweep angle
* C_{L_α} increases with increasing Mach number

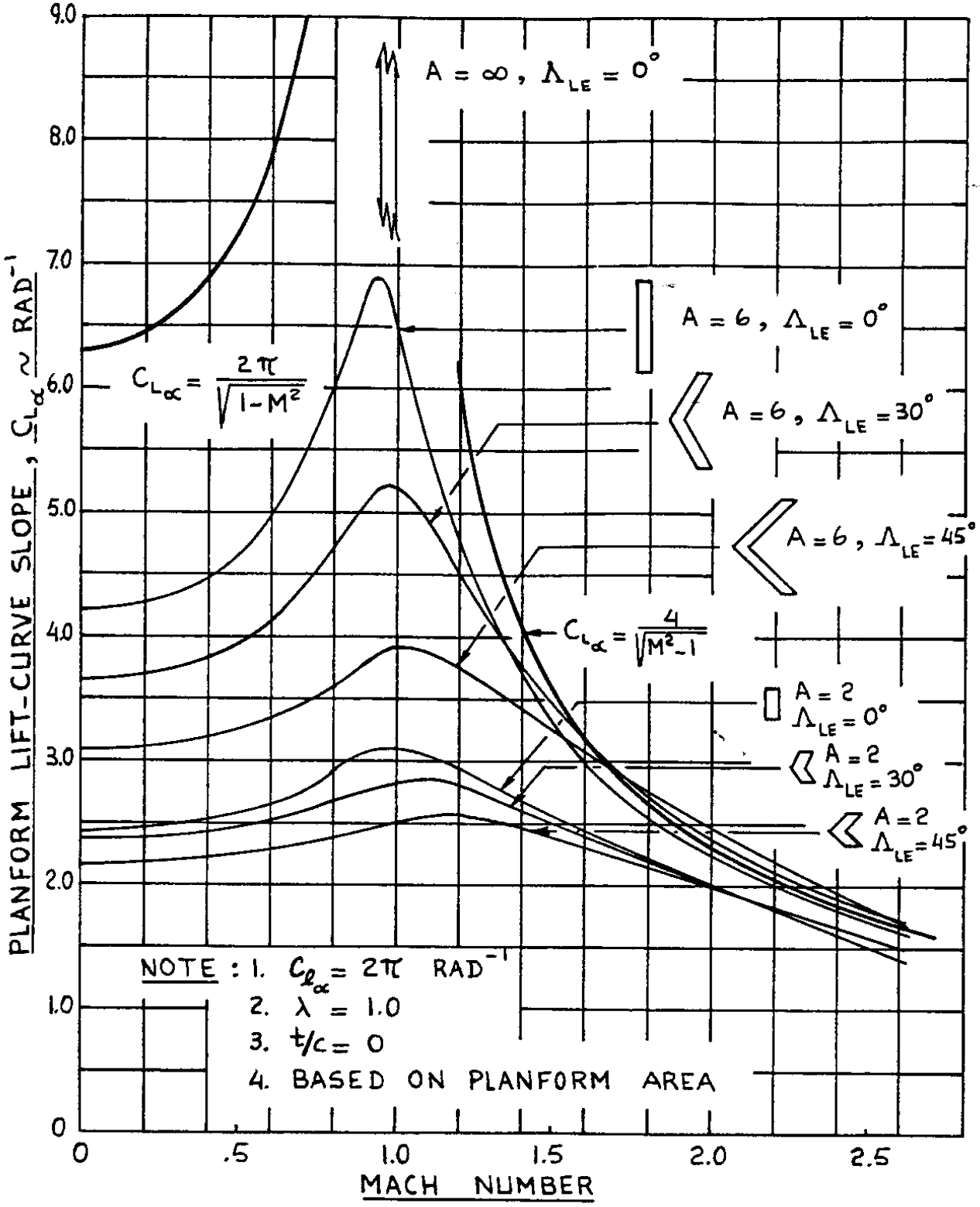

Figure 2.7 Effect of Mach Number and Planform Geometry on Lift-Curve Slope

Observe that below M=1.0 the trend of C_{L_α} with Mach number follows the Prandtl–Glauert transformation of Eqn (2.3).

In the supersonic speed range:

* C_{L_α} increases with increasing aspect ratio
* C_{L_α} tends to follow the supersonic Prandtl–Glauert transformation Eqn (2.5). Note that sweep angle does not matter very much in that speed range.

When estimating planform values for lift–curve slope it is a good idea to perform a 'sanity' check on the answers by comparing with Figure 2.7.

2.5.2 AERODYNAMIC CENTER

Definition: the aerodynamic center of a planform is defined as that point about which the pitching moment coefficient with angle of attack is in variant: $C_{m_\alpha} = 0$.

The planform aerodynamic center will be assumed to be located on its mean geometric chord (mgc). For planforms with moderate sweep angle and moderate to high aspect ratios the aerodynamic center is often close to the 25% chord point on the mgc. For other points on the mgc, the variation of pitching moment coefficient with angle of attack may be found from:

$$C_{m_\alpha} = C_{L_\alpha}(x_{ref} - x_{ac})\frac{1}{\bar{c}} = C_{L_\alpha}(\bar{x}_{ref} - \bar{x}_{ac}) \qquad (2.23)$$

The geometric definition of the parameters x_{ref} and x_{ac} is given in Figure 2.8. This figure also shows a simple geometric construction which can be used to determine the location of the mean geometric chord (mgc).

The aerodynamic center of a planform has been found to be primarily a function of the following parameters:

* Aspect ratio
* Sweep angle
* Taper ratio
* Section lift–curve slope
* Mach number

Methods for estimating planform aerodynamic center locations may be found in Part VI of Reference 2.3 (pages 305–308). Figure 2.9 shows an example of how the a.c. location varies with planform geometry. Until compressibility effects begin to play a role, it is seen that the planform aerodynamic center ranges from 25% to about 30% of the mgc. In the transonic speed range the aerodynamic center tends to move aft. For very thin wings, at supersonic speeds, the aerodynamic center moves close to the 50% chord point on the mgc. Figure 2.10 shows an example of how the aerodynamic center moves with sweep angle, taper ratio and Mach number.

For a given center of gravity location Eqn (2.23) suggests that the variation of pitching moment coefficient with angle of attack is strongly influenced by the location of the aerodynamic center. This will turn out to have a major influence on airplane controllability.

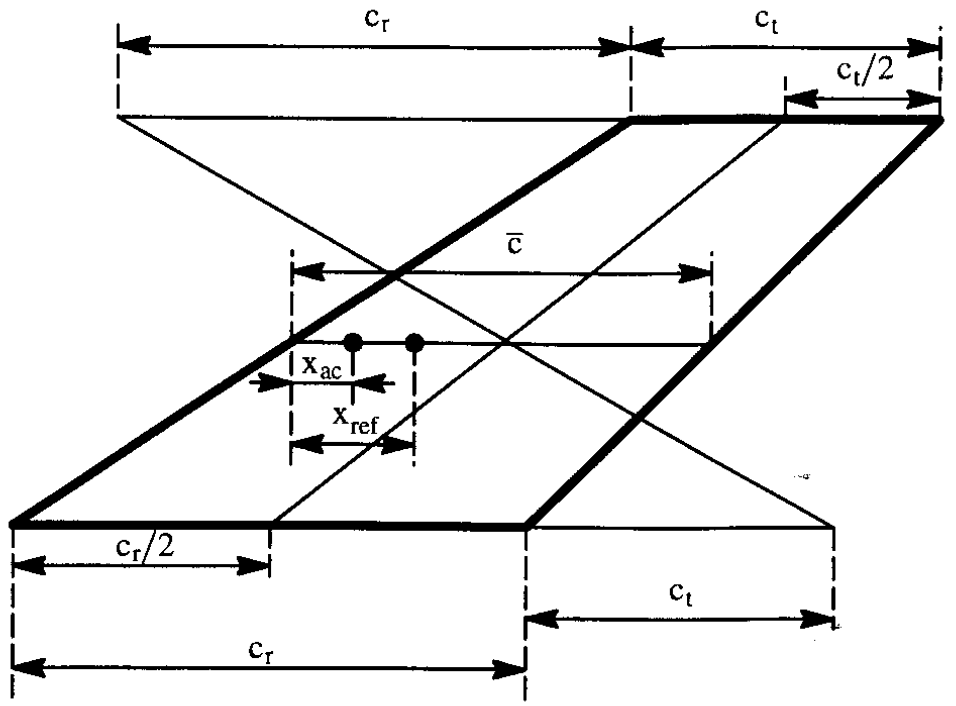

Figure 2.8 Definition of x_{ref} and x_{ac} and Construction of the MGC

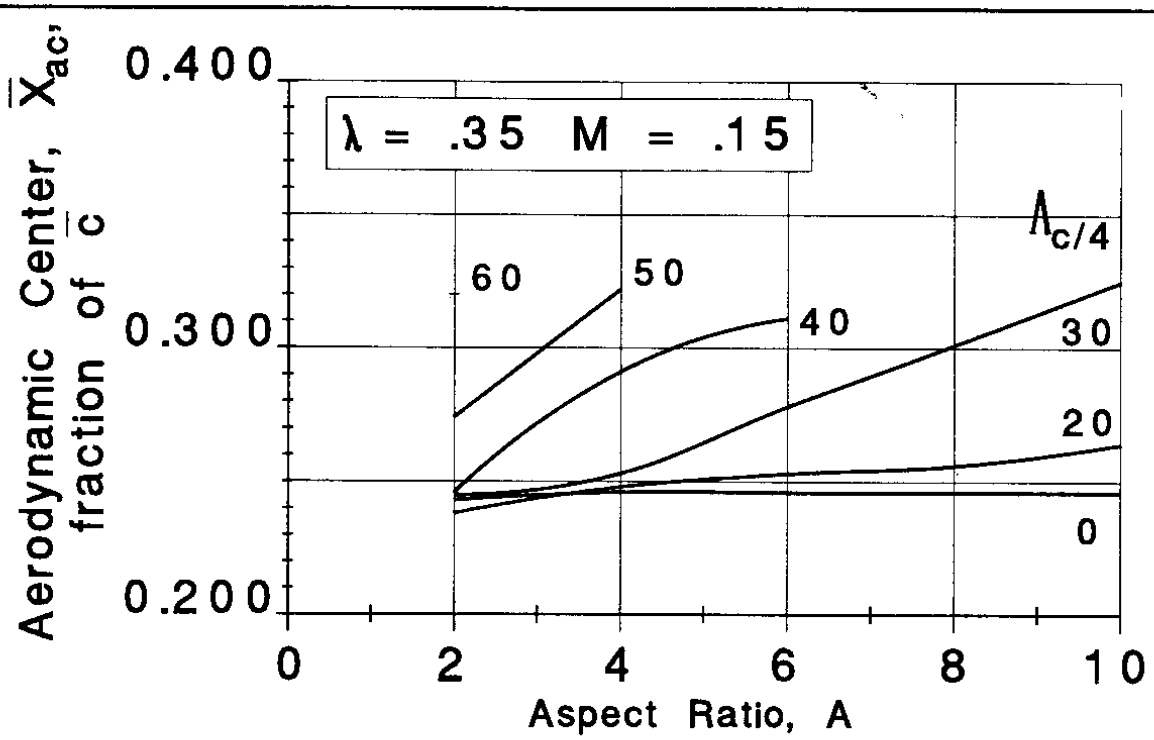

Figure 2.9 Effect of Planform Geometry on Aerodynamic Center (Subsonic)

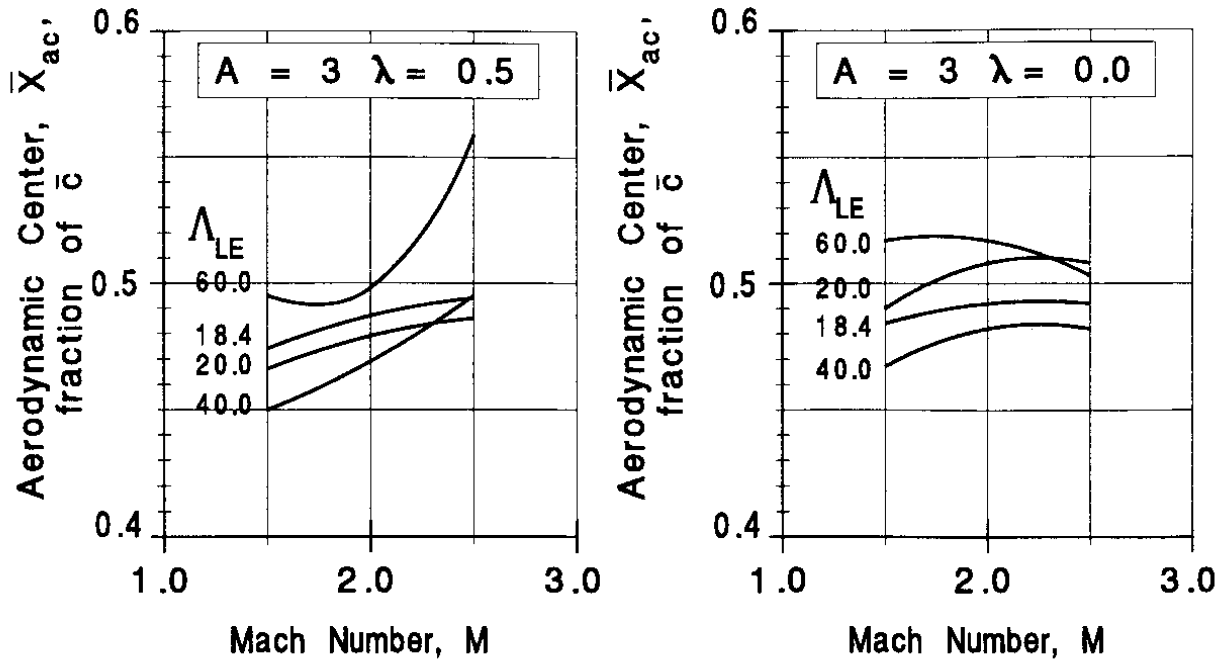

Figure 2.10 Effect of Planform Geometry on Aerodynamic Center (Supersonic)

2.5.3 ZERO–LIFT ANGLE OF ATTACK

The angle of attack of a planform is arbitrarily defined as the angle of attack of its root–chord. As the wording implies, the zero–lift angle of attack of a planform is that angle of attack for which the total planform lift equals zero. This quantity plays an important role in determining the required wing incidence angle for cruise and/or for approach flight conditions. The following parameters have been found to be instrumental in determining the zero–lift angle of attack of a planform:

* Aspect ratio
* Sweep angle
* Taper ratio
* Airfoil zero–lift angle of attack
* Planform twist

The planform twist angle at a given spanwise station, y, $\varepsilon_T(y)$ is defined in Figure 2.11. Note, that positive twist is defined as leading edge UP. Wings are typically twisted leading edge down at outboard wing stations to prevent the tip from stalling before the root. Another reason for twisting wing planforms is to tailor the spanwise load distribution such as to achieve certain induced drag or air–load distribution objectives.

The root angle of attack for which zero lift occurs at an intermediate span station, y is found from:

$$\alpha_{r_{l=0 \text{ at } y}} = \alpha_0(y) - \varepsilon_T(y) \tag{2.24}$$

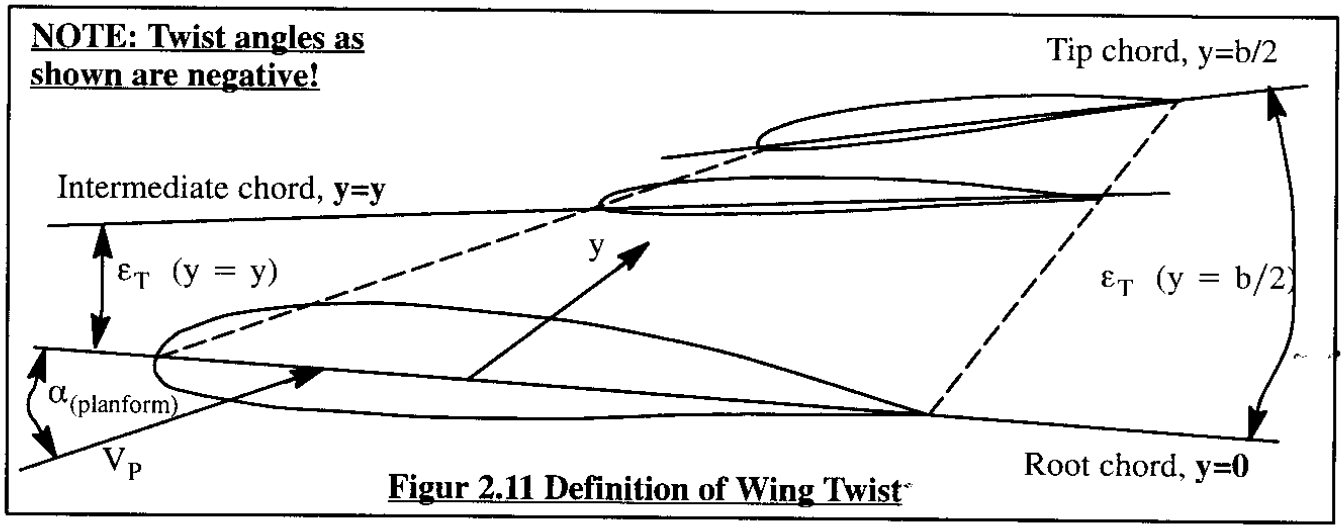

Figur 2.11 Definition of Wing Twist

By integrating this quantity over the planform, the value of planform angle of attack for zero planform lift is found as:

$$\alpha_{0_L} = \frac{1}{S}\int_{-b/2}^{b/2} c(y)[\alpha_0(y) - \varepsilon_T(y)]dy \tag{2.25}$$

This equation applies only to wings without sweep. When flaps are present anywhere along the span, their deflection can cause a significant shift in the planform angle of attack for zero lift. Methods for computing the effect of sweep and flaps on α_{0_L} are found in Part VI of Reference 2.3 (pages 245–247).

2.5.4 MOMENT COEFFICIENT ABOUT THE AERODYNAMIC CENTER

The pitching moment about the aerodynamic center of a wing has significant consequences for the trimmability of an airplane. In Sub–section 2.2.1 it was seen that positively cambered airfoils tend to have negative pitching moments about their aerodynamic centers (See Table 2.2). A planform consisting of positively cambered airfoils can therefore be expected to also have a negative value for its pitching moment coefficient about the aerodynamic center: $C_{m_{ac}}$. Methods for determining $C_{m_{ac}}$ for various planforms and Mach numbers are found in Part VI of Reference 2.3. It is noted that the value of $C_{m_{ac}}$ of a planform is the same as the pitching moment coefficient for zero lift (not zero angle of attack!), $\overline{C}_{m_0}$: see Eqn (2.3) where this is stated for airfoils. For a swept wing, the value of $C_{m_{ac}}$ is a strong function of the sweep angle, the spanwise twist distribution and the spanwise variation of airfoil zero–lift angle of attack. This can be seen from the following equation:

$$C_{m_{ac}} = \frac{1}{S\bar{c}}\left[\int_{-b/2}^{b/2} [c_{m_{ac}}(y)c(y)^2]dy + \pi\int_{-b/2}^{b/2} [\alpha_{0_L} + \varepsilon_T(y) - \alpha_0(y)]c(y)x_1(y)dy\right] \tag{2.26}$$

Figure 2.12 shows the definition of the geometric terms in Eqn (2.26).

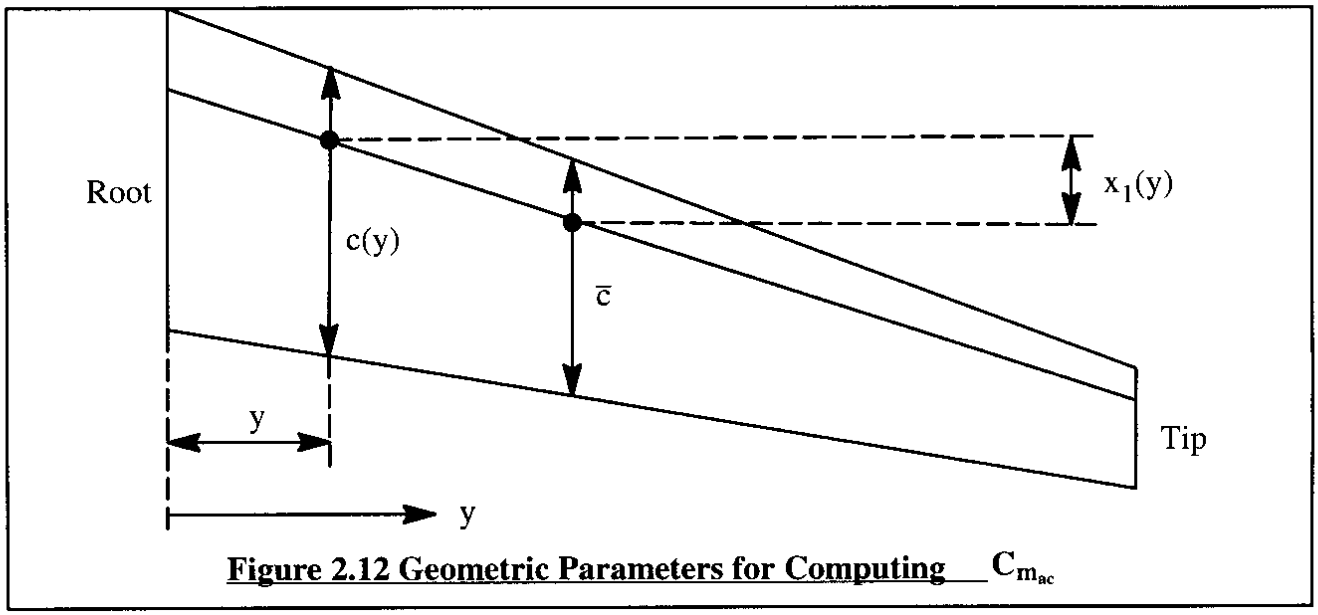

Figure 2.12 Geometric Parameters for Computing $C_{m_{ac}}$

2.5.5 DOWNWASH, UPWASH AND DYNAMIC PRESSURE RATIO (Adapted from Reference 2.4)

In Subsonic Flow

The downwash behind a wing is a consequence of the wing trailing vortex system. A typical wing trailing vortex system is pictured in Figure 2.13. A vortex sheet is shed behind the lifting wing. This vortex sheet is deflected downward (downwash) by the bound (or lifting) vortex and by the tip vortices which together comprise the wing vortex system. In general, the vortex sheet will not be flat although the curvature around the mid–span area is very small for large span wings. This is particularly true for high aspect ratio, low sweep angle wings. For such wings it has been found that considering the vortex sheet to be approximately flat is a good approximation. Wings with considerable trailing edge sweep angles tend to produce a vortex sheet which is bowed upward near the plane of symmetry.

The tip vortices normally do not experience a vertical displacement of the same magnitude as the central portion of the vortex sheet. In general they trail back comparatively close to the streamwise direction. Furthermore, as the vortex system moves downstream, the tip vortices tend to move inboard. Also, with increasing distance behind the wing, the trailing–sheet vorticity tends to be transferred to the tip vortices. This transfer of vorticity and the inboard movement of the tip vortices takes place in such a way that the lateral center of gravity of the vorticity remains at a fixed spanwise location. When all of the vorticity of the trailing–sheet has been transferred to the tip vortices, the vortex system is considered top be fully rolled –up. In a non–viscous fluid this vortex system would extend to infinity. This way of looking at the vortex system is consistent with the vortex laws formulated by Helmholtz (See Ref. 2.5.).

Ahead of the downstream station of complete roll–up, the spanwise downwash distribution is dependent on the spanwise lift distribution of the wing. However, when the roll–up is complete, the downwash angles for all planforms of equal lift and equal effective span are identical!

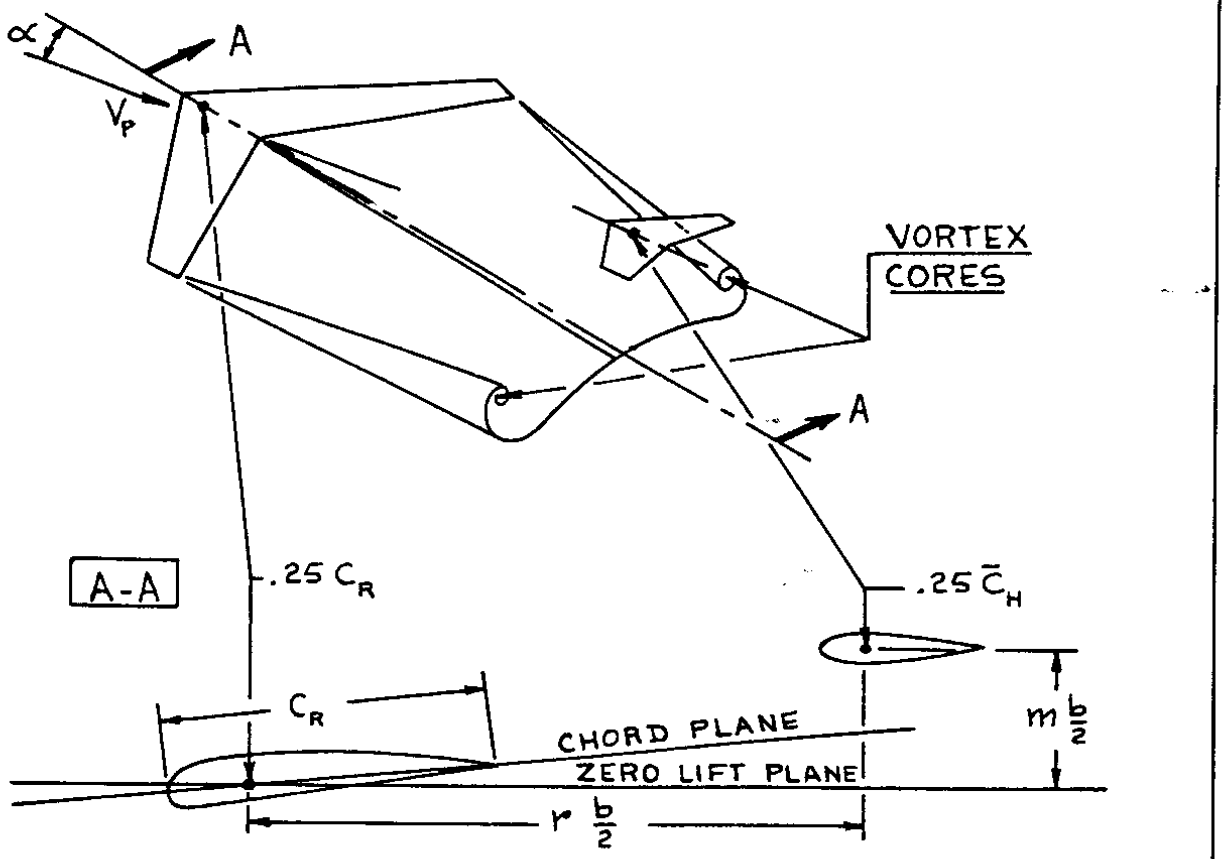

Figure 2.13 Geometry for Downwash Determination

As suggested by Figure 2.13, the shape of the vortex sheet will have a significant effect on the downwash experienced by a horizontal tail placed in the flow field behind a wing. The location of such a tail (vertical and horizontal) relative to the wing is therefore very important. Because the wing–tip vortices are somewhat above the wing vortex sheet, the downwash above the sheet is somewhat larger than the downwash below the vortex sheet. The rate at which the downwash angle changes with angle of attack is the so–called downwash gradient, $d\varepsilon/d\alpha$. The numerical value of this downwash gradient in the zero–lift plane ranges from 1.0 at the wing trailing edge to $2C_{L_\alpha}/\pi A$ at infinity. Figure 2.14 shows an example of how the downwash gradient varies for various horizontal tail locations behind an unswept wing of different aspect ratios.

In stability considerations (as shown in Chapter 3) the parameter $(1 - d\varepsilon/d\alpha)$frequently occurs. Figure 2.15 shows how this parameter varies for locations in front of and behind wings with elliptical planforms. In front of the wing the term upwash is used instead of downwash. Upwash is particularly important in the case of canard airplanes.

In subsonic flow the downwash gradient tends to vary with Mach number as predicted by the Prandtl–Glauert transformation:

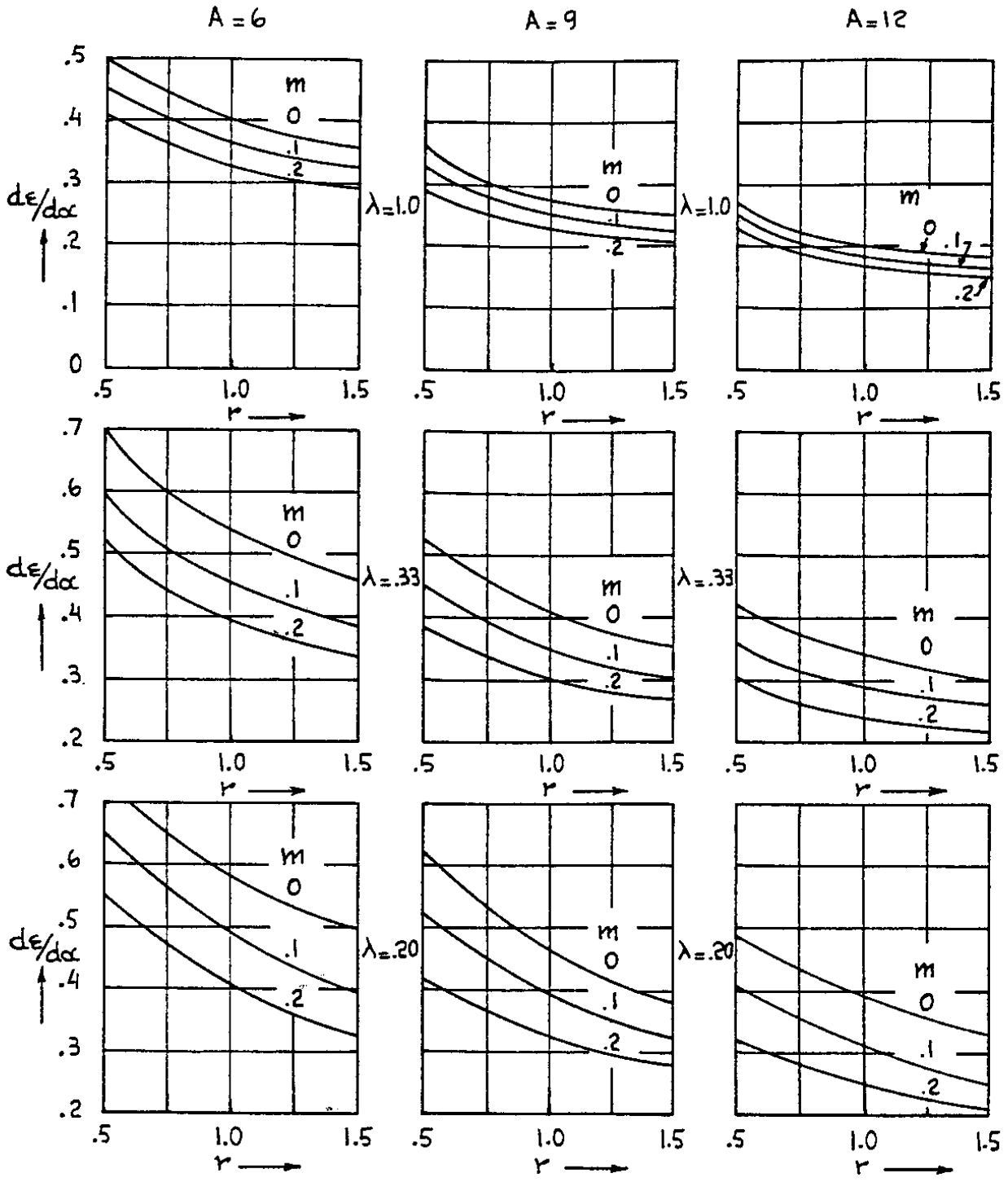

Notes: 1. Valid only for straight, tapered wings at low Mach Numbers
2. For other aspect ratios, interpolate or extrapolate
3. See Part VI of Reference 2.3 for a more general method

$$m = \frac{\text{Vertical distance of horizontal tail } 0.25\bar{c}_h \text{ above/below the wing zero lift line}}{b/2}$$

$$r = \frac{\text{Longitudinal distance of } 0.25c_r \text{ toward the horizontal tail } 0.25\bar{c}_h \text{ location}}{b/2}$$

Figure 2.14 Effect of Wing Aspect Ratio and Horizontal Tail Location on the Downwash Gradient

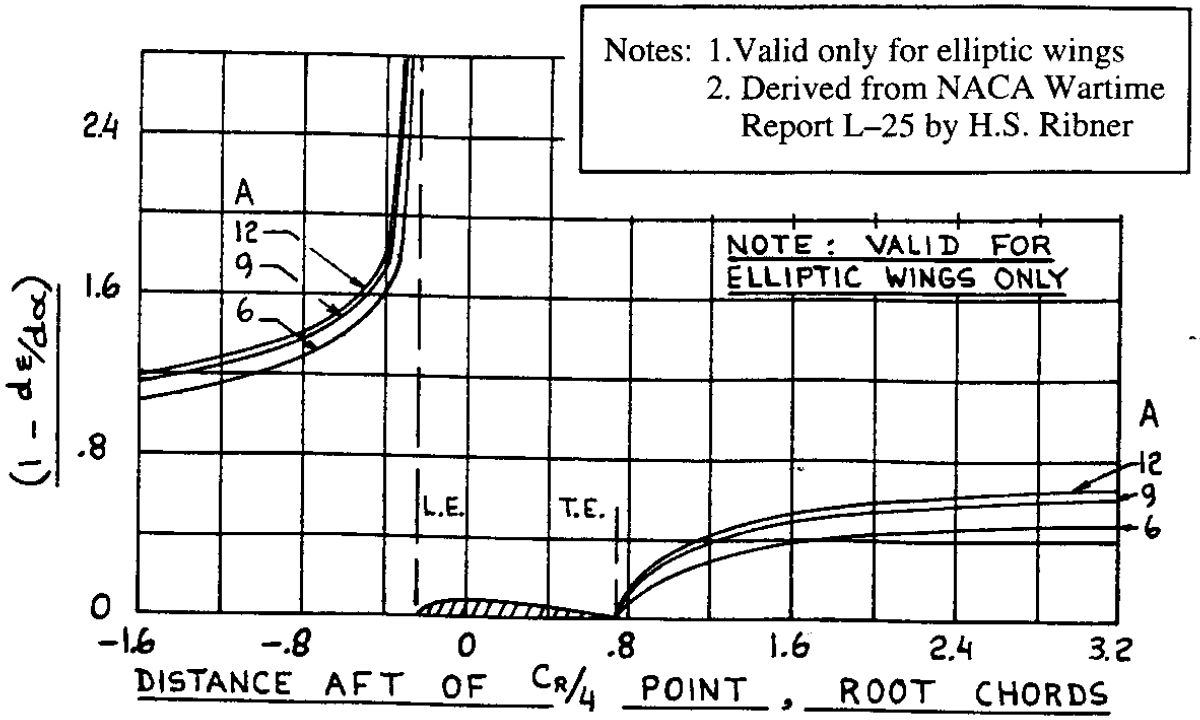

Figure 2.15 Magnitude of $(1 - d\varepsilon/d\alpha)$ on the Longitudinal Axis

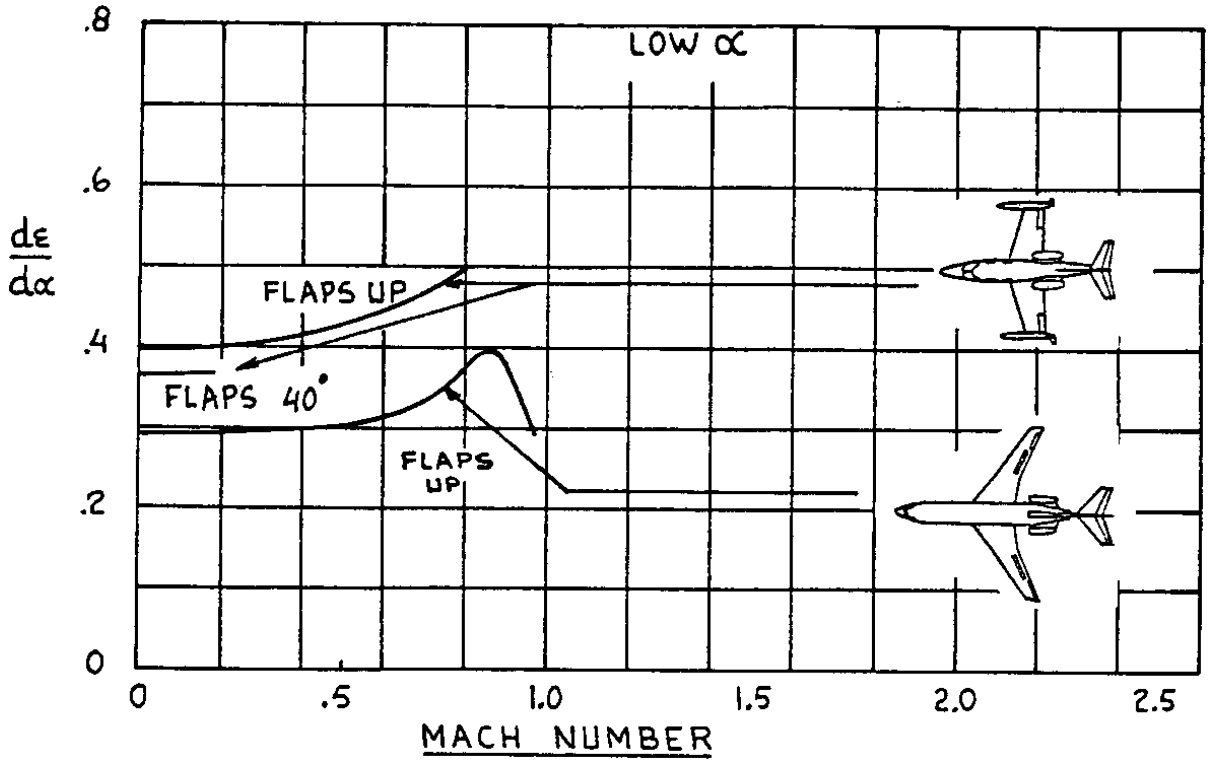

Figure 2.16 Examples of Variation of $d\varepsilon/d\alpha$ with Mach Number

$$(d\varepsilon/d\alpha)_M = (d\varepsilon/d\alpha)_{M=0}\sqrt{(1 - M^2)} \tag{2.27}$$

A method for calculating the downwash gradient behind arbitrary wings is given in Part VI of Reference 2.3. Figure 2.16 shows an example of how the downwash gradient varies with Mach number for several airplanes.

In the case of low aspect ratio wings and in the case of a canard configuration the tip vortex of the wing or the canard may impinge on the the aft surface. Reference 2.7 contains a method to account for that.

Upwash is induced ahead of a wing in a manner similar to that for downwash. To account for the aerodynamic forces on propellers, nacelles and/or stores ahead of a wing due to this upwash the design charts of Reference 2.7 may be used.

Dynamic Pressure Ratio

The aerodynamic forces on lifting surfaces are proportional to the local dynamic pressure of the flow field. The reference (or free stream) dynamic pressure used in computing aerodynamic forces and moments on the entire airplane is that based on airplane true air speed: $\bar{q} = 0.5\rho V_P^2$. The dynamic pressure in the downwash wake of a wing can be reduced by friction losses and/or by separation phenomena. However, if an aft surface is mounted in the propeller wake it is possible that (depending on engine power) the dynamic pressure is in fact larger than the free–stream dynamic pressure. The change in local dynamic pressure is expressed in terms of a ratio of dynamic pressures. For example, in the case of horizontal and vertical tails these ratios are expressed as: $\eta_h = \bar{q}_h/\bar{q}$ and $\eta_v = \bar{q}_v/\bar{q}$ respectively. Part VI of Reference 2.3 (Pages 269–271) contains methods for estimating these dynamic pressure ratios.

In Transonic Flow

In transonic flow no accurate methods are available as yet to estimate downwash characteristics. When estimates (or tunnel data) are available for wing lift–curve slope in the transonic region, a first order approximation for estimating the downwash gradient is to use the lift–curve slope ratio:

$$(d\varepsilon/d\alpha)_M = (d\varepsilon/d\alpha)_{M=0}\frac{C_{L_{\alpha_M}}}{C_{L_{\alpha_{M=0}}}} \tag{2.28}$$

In Supersonic Flow

At supersonic speeds downwash is caused by two factors. First, the region behind the trailing–edge shock or expansion wave is distorted by the wing vortex system in a manner similar to that which occurs at subsonic speeds. Because of the variation of span load, a vortex sheet is shed which rolls up with increasing downstream distance from the trailing edge. Tip vortices similar to their subsonic counterparts are also present. At supersonic Mach numbers the entire flow field is swept back and isolated regions of influence may exist over certain portions of the wing surface and in the

flow field behind it. For instance, regions not affected by the wing tip are generally present.

Second, a change in flow direction occurs in the flow region between the leading edge shock or expansion waves as shown in Figure 2.17. Since this region of the flow does not 'see' the wing vortex system, numerical values for downwash can be calculated with shock–expansion theory. To simplify the calculations it is standard practice to perform these calculations with the geometry of the wing root and to assume two–dimensional flow. For configurations where the tail span is less than the wing span, this assumption is justified.

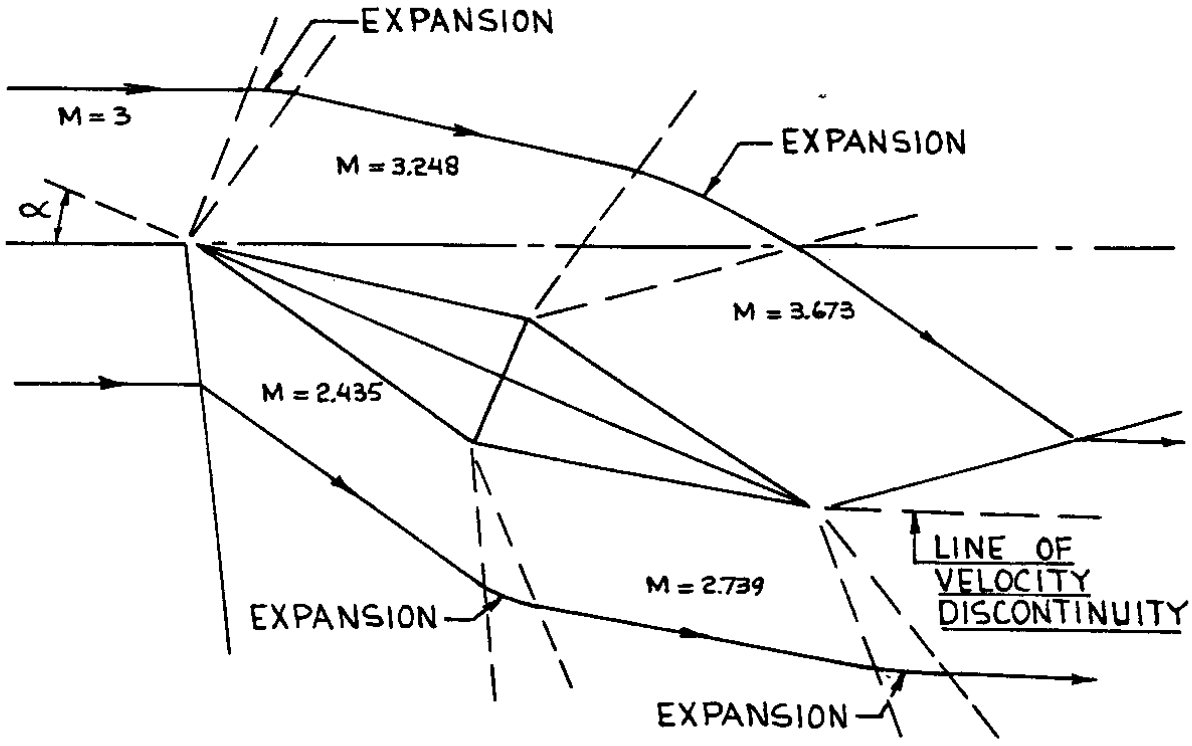

Figure 2.17 Shock Distribution on a Wedge Airfoil in Supersonic Flow

2.5.6 EFFECT OF THE FUSELAGE ON WING AERODYNAMIC CENTER

When a fuselage is added to a wing, the aerodynamic center of the wing+fuselage shifts forward compared to that of the wing alone. A physical explanation for this effect can be seen from Figure 2.18. Considering the fuselage to be represented by a body of revolution placed in a potential flow field the pressure distribution is roughly as indicated by the + and – signs in Figure 2.19.

In potential flow, at a given angle of attack, α the following observations can be made:

*** net pressure drag is zero** *** net lift is zero** *** net pitching moment is positive.**

As a consequence the fuselage will add a positively increasing pitching moment with each increase of angle of attack: the fuselage adds an increment $\Delta C_{m_{\alpha_{fus}}} > 0$ to the wing. This increment

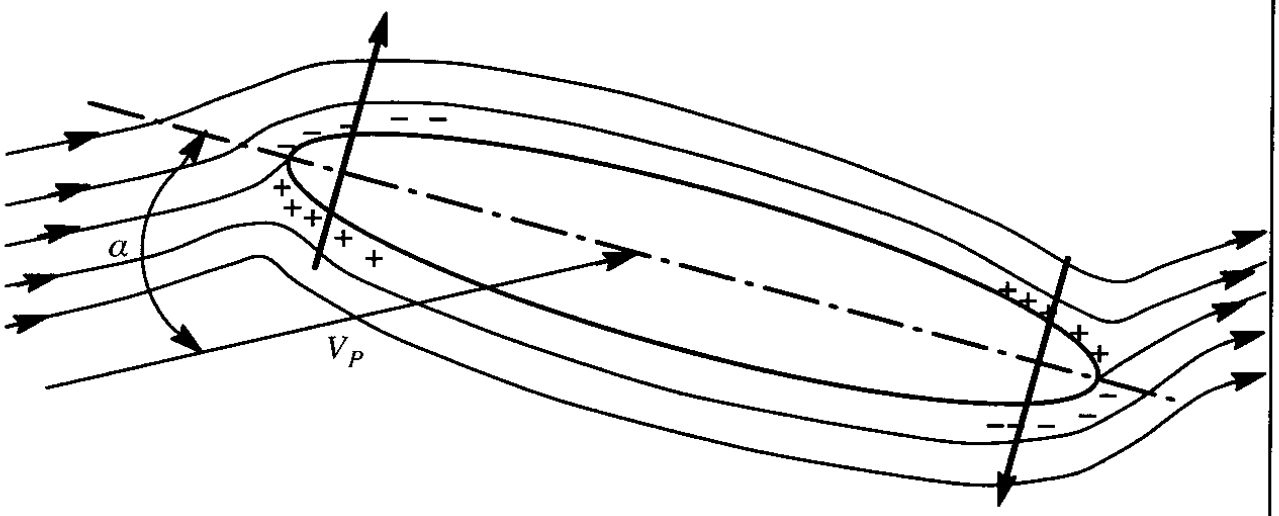

Figure 2.18 A Body of Revolution in Potential Flow at Angle of Attack

in the static longitudinal stability derivative, C_{m_α} can be interpreted as a forward shift in aerodynamic center: $\Delta\bar{x}_{ac_{fus}}$ which is negative. This fuselage effect is also called the Munk effect (after its discoverer, Max Munk). Part VI of Reference 2.3 contains a numerical integration method for estimating the fuselage induced shift of the aerodynamic center. This method accounts for the effect of wing up–wash and wing down–wash on the fuselage. It is based on a method first developed by Multhopp in Reference 2.10.

Figure 2.19 shows three numerical examples of this fuselage induced a.c. shift as computed for different airplanes. It is shown in Part II of Reference 2.3 that typical center–of–gravity shifts in airplanes range from 10%–25% of the mgc. The 4%, 14% and 32% fuselage induced shifts in aerodynamic center location are therefore very important and must be accounted for in the design of a new airplane!

It has been found that the fuselage induced a.c. shift is essentially independent of Mach number for moderate to high fuselage slenderness ratios. Therefore, the aerodynamic center of a wing+fuselage tends to shift aft with Mach number more or less like that of a wing alone.

It should be noted that nacelles and stores when mounted under a wing such that they protrude forward from the wing leading edge, also cause a shift in a.c. These shifts can also be predicted with the Multhopp method.

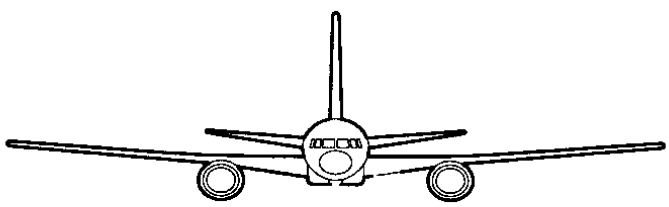

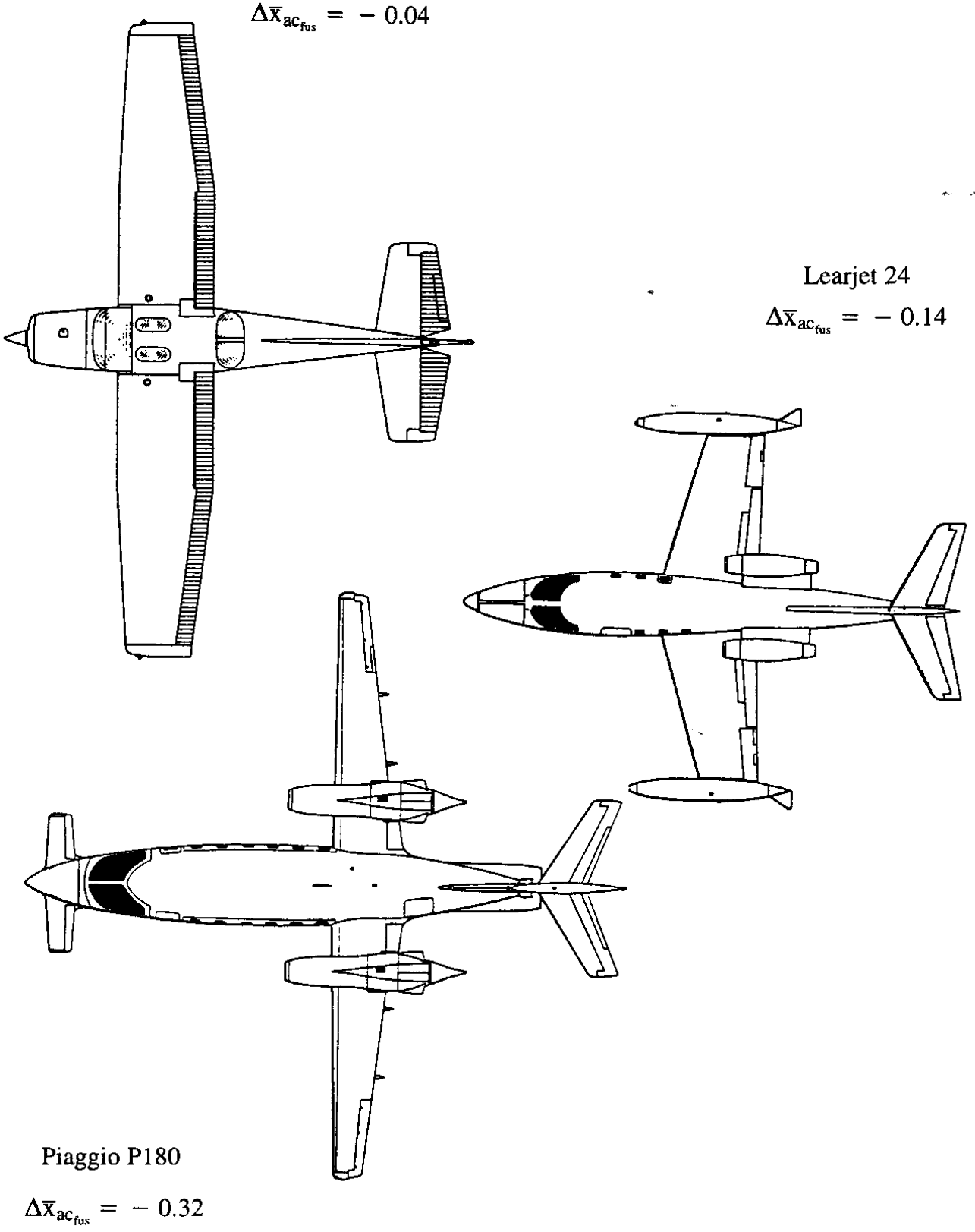

Figure 2.19 Numerical Examples of Fuselage Induced Shift in Aerodynamic Center

2.6 EFFECTIVENESS OF CONTROL SURFACES

The controllability of airplanes depends on the lift and moment effectiveness of flight control surfaces. Most control surfaces are designed as plain flaps (with open or closed gap) as illustrated in Figure 2.20. Closed gap configurations have greater effectiveness than open gap configurations. Note that a control surface deflection **is defined as positive** when the trailing edge is down.

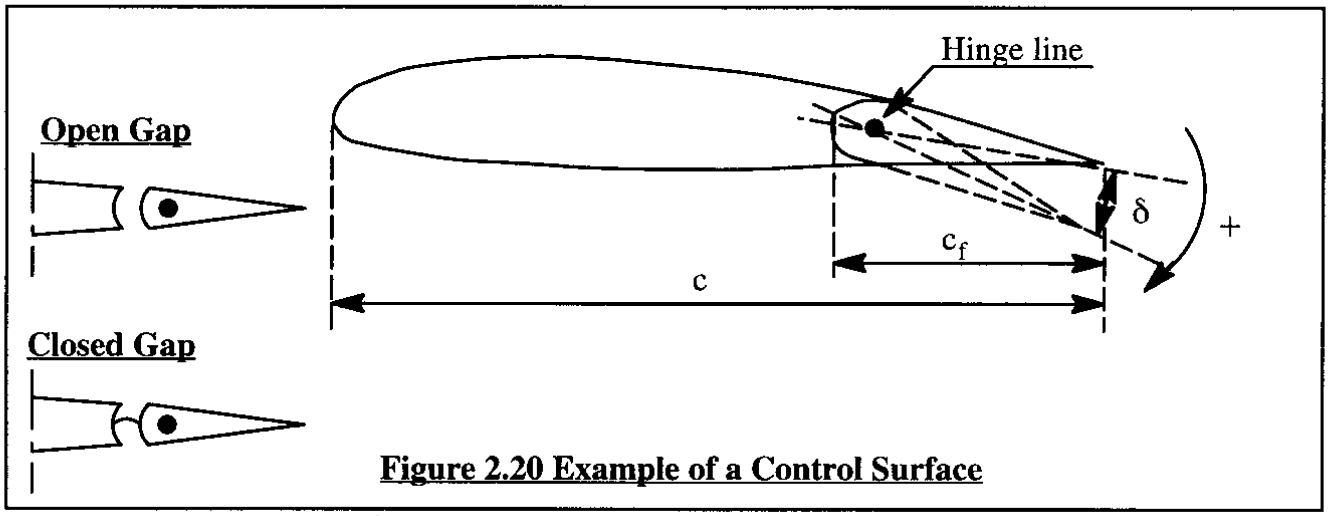

Figure 2.20 Example of a Control Surface

The lift effectiveness of a control surface is designated by $c_{l_\delta} = \frac{\partial c_l}{\partial \delta}$ for an airfoil and $C_{L_\delta} = \frac{\partial C_L}{\partial \delta}$ for a planform. For an airfoil section, the magnitude of c_{l_δ} depends primarily on the following parameters:

* control surface chord ratio, c_f/c
* section thickness ratio, t/c
* control surface deflection, δ
* Mach number

Figure 2.21 shows an example of how c_{l_δ} depends on the first two parameters. It is seen that the chord ratio has primary influence while the thickness ratio has only secondary influence on lift effectiveness. It will be shown in Chapter 3 that in most airplane control power derivatives the lift effectiveness appears in product form with the moment arm of the control surface to the center of gravity. Methods for estimating C_{L_δ} from c_{l_δ} are found in Part VI of Reference 2.3. Factors which affect the numerical magnitude of C_{L_δ} are, in addition to those mentioned for c_{l_δ} :

* Sweep angle
* Control surface inboard and outboard span stations, η_i and η_o

The latter two quantities are defined in Figure 2.6. Figure 2.22 shows a typical plot of planform lift versus angle of attack, cross–plotted for control surface deflections. It is important to understand the graphical interpretation for C_{L_δ} :

$$C_{L_\delta} = \left(\frac{\partial C_L}{\partial \delta}\right)_{\alpha = \text{constant}} \tag{2.29}$$

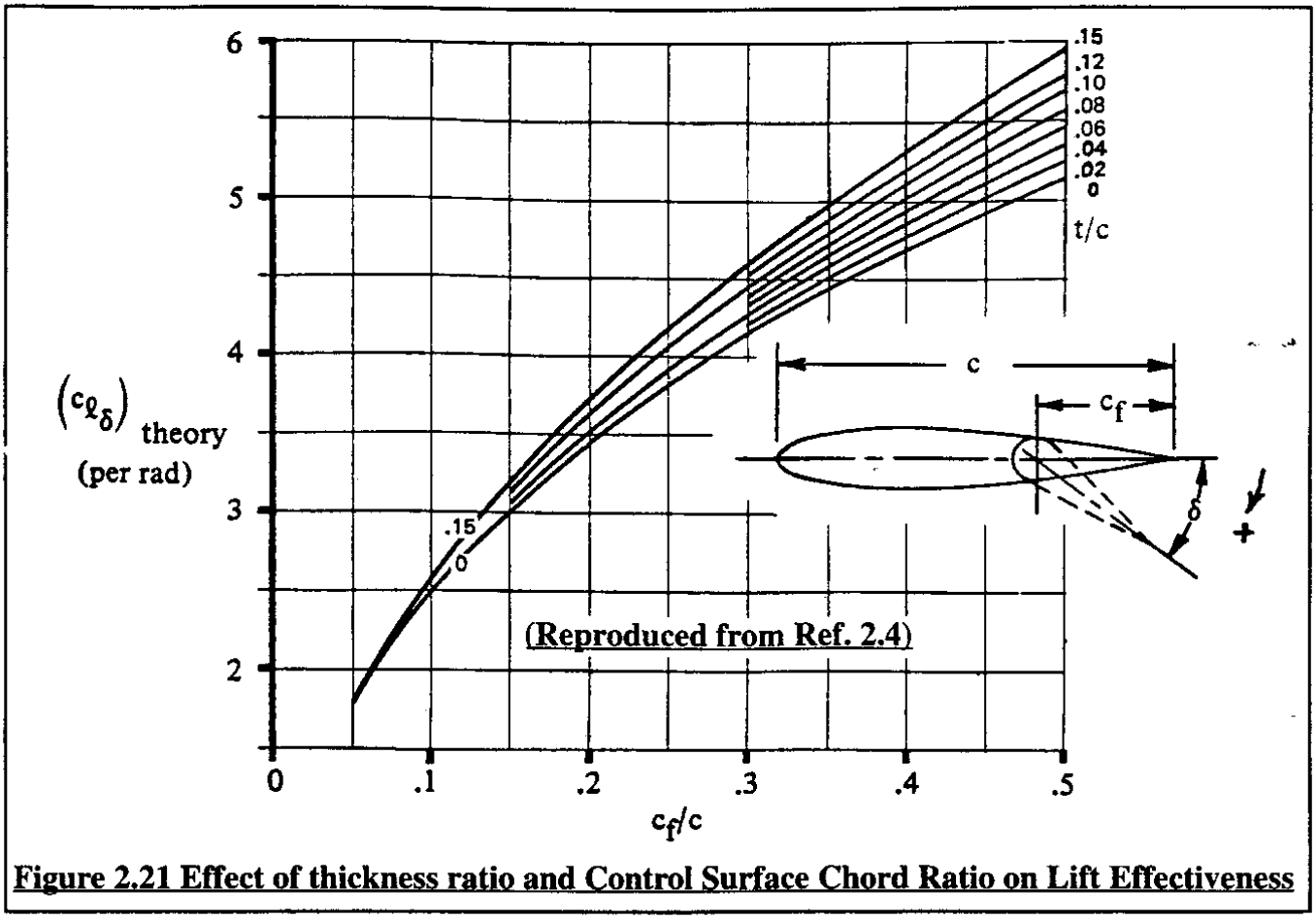

Figure 2.21 Effect of thickness ratio and Control Surface Chord Ratio on Lift Effectiveness

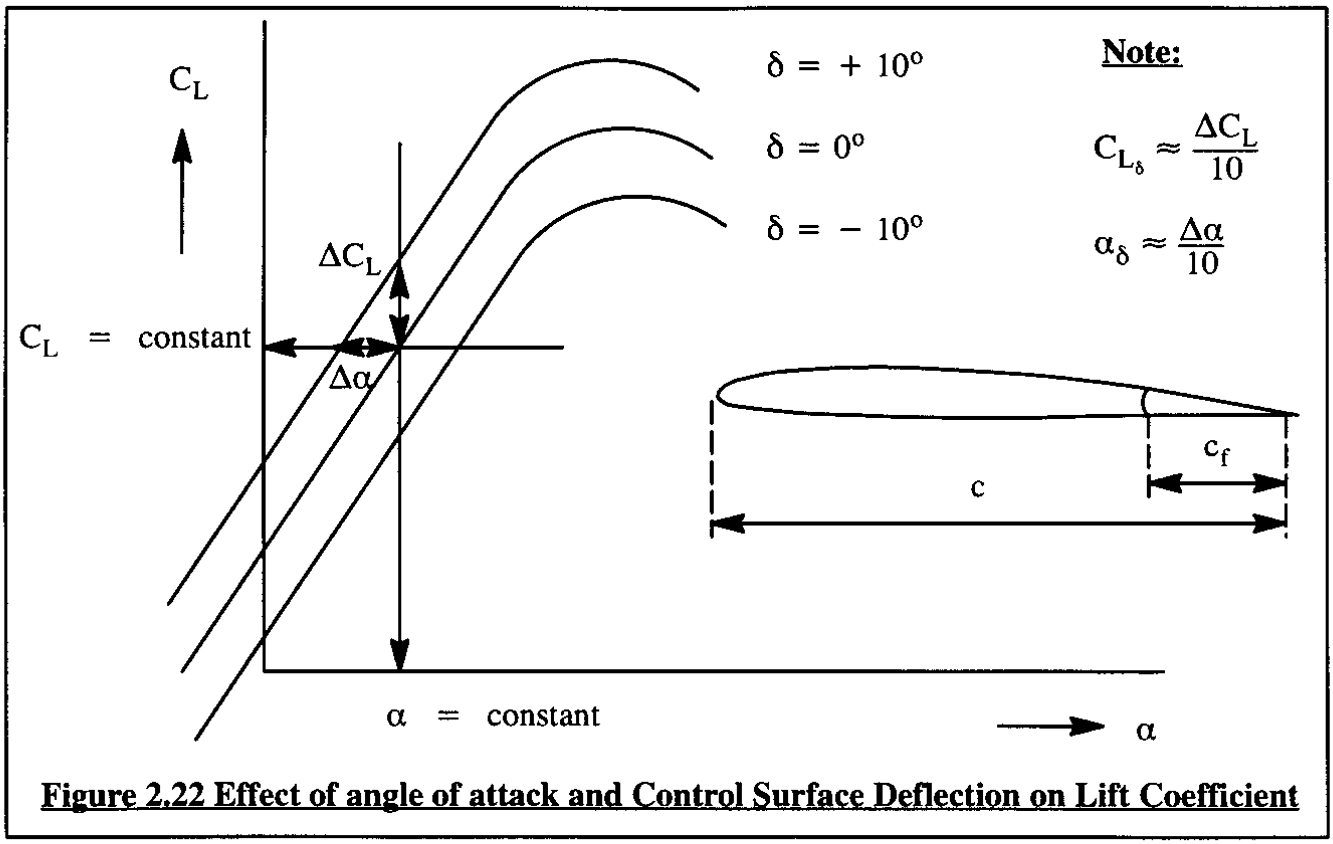

Figure 2.22 Effect of angle of attack and Control Surface Deflection on Lift Coefficient

This quantity can be viewed as the change in lift coefficient due to control surface deflection at constant angle of attack. In many stability and control expressions in Chapter 3 the following quantity (called angle–of–attack effectiveness) is also important:

$$\alpha_\delta = \left(\frac{\partial \alpha}{\partial \delta}\right)_{C_L = \text{constant}} \tag{2.30}$$

This quantity can be viewed as the change in angle of attack due to control surface deflection at constant lift coefficient. It may be seen that as long as $\alpha < \alpha^*$ the following holds:

$$\alpha_\delta = \frac{C_{L_\delta}}{C_{L_\alpha}} \tag{2.31}$$

Figure 2.23 shows how α_δ varies with c_f/c. It is seen that a control surface with a 30% chord has 50% of the effectiveness of an all–moving (100% chord or variable incidence) planform. This is the reason why hinged control surfaces have been used on so many airplanes: per unit chord length they are very effective!

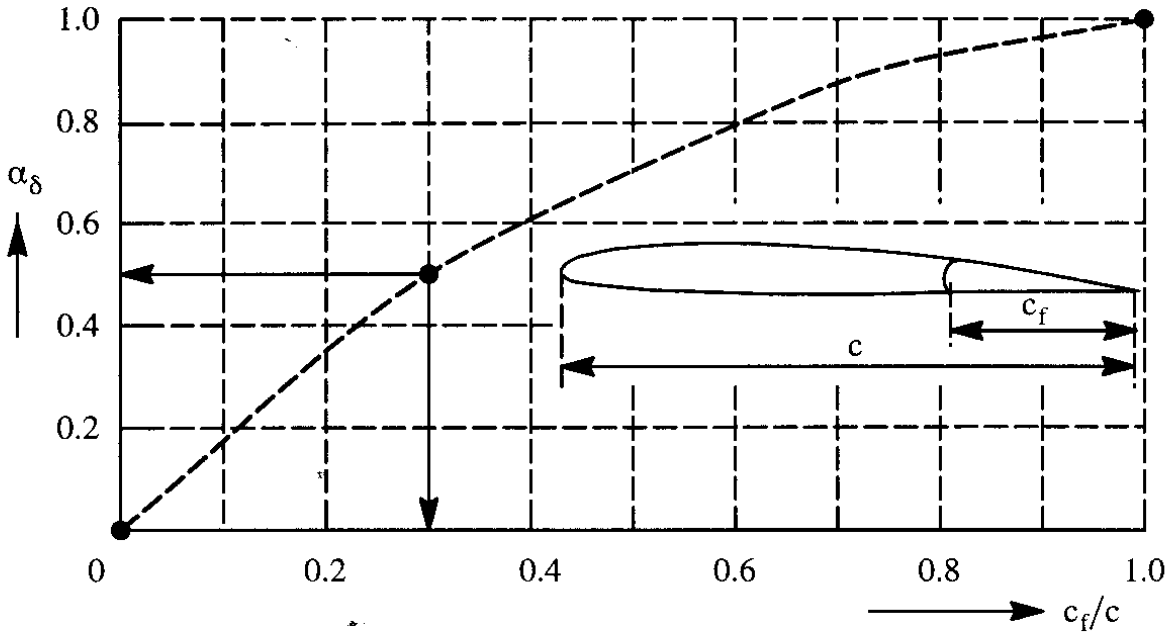

Figure 2.23 Effect of Control Surface Chord Ratio on α_δ

For a three–dimensional control surface at very low sweep angles, a good approximation for α_δ is:

$$\alpha_\delta = \frac{1}{S}\int_{-b/2}^{b/2} \alpha_\delta(y)c(y)dy \tag{2.32}$$

For variations with Mach number in subsonic flow, the Prandtl–Glauert transformation can be used again to yield:

$$c_{l_\delta} = \frac{c_{l_{\delta M=0}}}{\sqrt{1 - M^2}} \qquad \text{and} \qquad C_{L_\delta} = \frac{C_{L_{\delta M=0}}}{\sqrt{1 - M^2}} \tag{2.33}$$

More general methods which account for the effect of sweep angle and for transonic and super sonic flow are found in Part VI of Reference 2.3.

2.7 MODERN AIRFOILS COMPARED TO NACA AIRFOILS

Since the advent of reliable computational methods for the prediction of airfoil behavior and for the design of airfoils (for example, References 2.8 and 2.9) it is possible to develop airfoils with lift, drag and pitching moment characteristics which are tailored to specific applications and specific flight conditions. Figure 2.24 shows a geometric comparison between older and newer airfoils. Figure 2.25 show example data comparing modern airfoils with NACA type airfoils.

2.8 SUMMARY FOR CHAPTER 2

In this chapter the following airfoil, planform, fuselage and control surface aerodynamic properties which are important to the stability and control of airplanes were reviewed:

* Lift–curve slope
* Zero–lift pitching moment coefficient
* Fuselage induced aerodynamic center shift
* Zero–lift angle of attack
* Aerodynamic center
* Control surface lift effectiveness

In addition, a number of important geometric characteristics of planforms were introduced.

Most of the quantities mentioned in this chapter can be rapidly evaluated with the AAA program described in Appendix A.

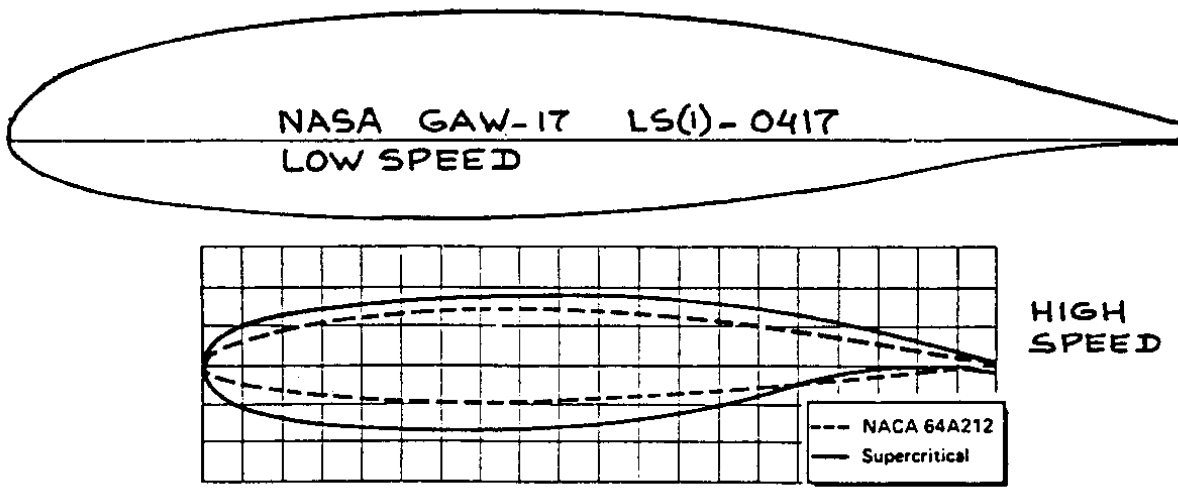

Figure 2.24 Geometric Comparison of Modern and NACA Airfoils

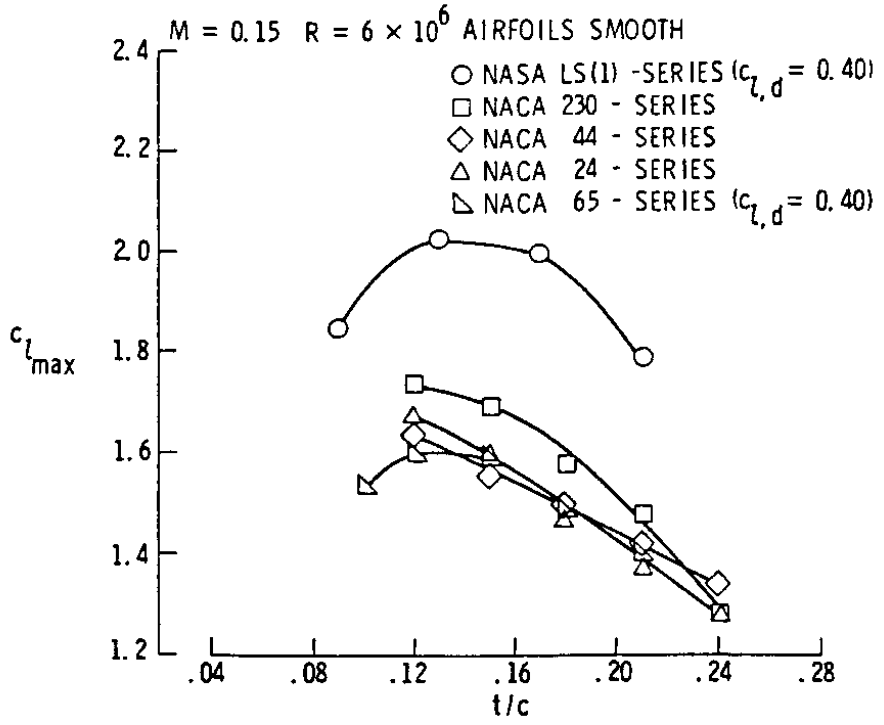

Figure 2.25 Comparison of Maximum Lift Capability of Modern and NACA Airfoils

2.9 PROBLEMS FOR CHAPTER 2

2.1 For a thin airfoil, calculate and plot the theoretical section lift–curve slope for $0 < M < 2.0$.

2.2 Using data from Reference 2.2 plot section lift–curve slope versus thickness ratio for NACA 44XX and 23YYY series airfoils.

2.3 Make accurate sketches of wing planforms, characterized by the following parameters:
Leading edge sweep angle: 0 degrees:

a) $\lambda = 0$ A = 2, 4, 6, 8, 10
b) $\lambda = 0.35$ A = 2, 4, 6, 8, 10
b) $\lambda = 1.0$ A = 2, 4, 6, 8, 10
d) $\lambda = 1.35$ A = 2, 4, 6, 8, 10

Repeat this assignment for leading edge sweep angles of 30 and 60 degrees.

2.4 Consult recent and older versions of Jane's All The World Aircraft to find examples of air–planes with wings which approximately fit some of the planforms sketched in Problem 2.3.

2.5 Calculate and plot the planform lift curve slope versus Mach number for the following two families of wings:

Leading edge sweep angle: 0, 20, 40 and 60 degrees
Aspect ratio: 2, 6 and 10
Taper ratio: 0.35

Note: The method of Part VI of Ref.2.3 or any other suitable method can be used.

2.6 Calculate and plot the planform aerodynamic center location versus Mach number for the following two families of wings:

Leading edge sweep angle: 0, 20, 40 and 60 degrees
Aspect ratio: 2, 6 and 10
Taper ratio: 0.35

Note: The method of Part VI of Ref.2.3 or any other suitable method can be used.

2.10 REFERENCES FOR CHAPTER 2

2.1 Lan, C.E. and Roskam, J.; Airplane Aerodynamics and Performance; Design, Analysis and Research Corporation, 120 East Ninth Street, Suite 2, Kansas, 66064, USA; 1997.

2.2 Abbott, I.H. and Von Doenhoff, A.E.; Theory of Wing Sections; Dover Publications, N.Y.; 1959.

2.3 Roskam, J.; Airplane Design, Parts I through VIII; Design, Analysis and Research Corporation, 120 East Ninth Street, Suite 2, Lawrence, Kansas, 66044, USA; 1990.

2.4 Hoak, D.E. and Ellison, D.E. et al; USAF Stability and Control DATCOM; 1968 edition, Flight Control Division, Air Force Flight Dynamics Laboratory, Wright Patterson Air Force Base, Ohio.

2.5 Kuethe, A.M. and Schetzer, J.D.; Foundations of Aerodynamics; J. Wiley & Sons, New York, 1959.

2.6 Bonney, E.A.; Engineering Supersonic Aerodynamics; McGraw-Hill, New York, 1950.

2.7 Alford, W.J., Jr.; Theoretical and Experimental Investigation of the Subsonic Flow Fields Beneath Swept and Unswept Wings with Tables of Vortex-Induces Velocities; NACA TN 3738, August 1956.

2.8 Bauer, F., Garabedian, P. and Korn, D.; A Theory of Supercritical Wing Sections II; Lecture Notes in Economic and Mathematical Systems, Volume 108, Springer Verlag, N.Y., 1975.

2.9 Eppler, R. and Sommers, D.M.; A Computer Program for the Design and Analysis of Low Speed Airfoils, NACA TM-80210, 1980.

2.10 Multhopp, H.; Aerodynamics of the Fuselage; NACA Technical Memorandum No. 1036, December 1942.